Wave Run-up on a Highly Dissipative Beach

by

Carmen Holmes-Smith

B.Sc., University of Victoria, 2019

A Thesis Submitted in Partial Fulfillment of the
Requirements for the Degree of

MASTER OF SCIENCE

in the Department of Earth and Ocean Sciences

We acknowledge and respect the Lək̓ʷəŋən (Songhees and Esquimalt) Peoples on whose territory the university stands, and the Lək̓ʷəŋən and W̱SÁNEĆ Peoples whose historical relationships with the land continue to this day.

Wave Run-up on a Highly Dissipative Beach

by

Carmen Holmes-Smith

B.Sc., University of Victoria, 2019

Supervisory Committee

Dr. Johannes Gemmrich, Supervisor
Physics and Astronomy/School of Earth and Ocean Science

Dr. Jody Klymak, Supervisor
Physics and Astronomy/School of Earth and Ocean Science

Dr. Brad Buckham, Outside Member
Mechanical Engineering

Abstract

Long-term observations of wave run-up were collected using video imagery. The study site is a highly dissipative sand beach on the West Coast of Vancouver Island with seasonally energetic wave behaviour. Spectral analysis of the long-term timeseries was done to characterize the run-up spectrum. These run-up spectra consistently show a peak frequency in the infragravity range, with a frequency dependence of $f^{-1.5}$. This demonstrates a clear spectral shift of the characteristic developed wind-wave spectrum in deep water, which has a dominant period of approximately 10 seconds and a frequency dependence of f^{-4}. The spectral transformation is consistent with findings from previous run-up studies, although the peak period and frequency dependence of the spectra presented here show an extreme example of this expected spectral evolution. Additional instruments utilized in the analysis include an offshore wave buoy, a Spotter buoy deployed immediately outside the surf-zone, and for a shorter three week period, an RBR pressure sensor that was deployed on the same mooring as the Spotter buoy. Correlations were evaluated between run-up behaviour and sea-state variables to understand wave transformation across the surf-zone, as well as to find useful and practical indicators of heightened wave run-up hazard that can be used by risk managers. Significant wave height (Hs), dominant period (T0), and the parameter $\sqrt{HL}$ are all positively correlated to run-up extent, with $\sqrt{HL}$ being the strongest predictor. A positive correlation was also found between large run-up events and the amount of relative infragravity energy present in the incoming wave field. The process of bore-bore capture (BBC) was shown to be a likely mechanism behind the drastic spectral shift to lower peak frequencies. BBC was also shown to drive extreme run-up events, especially when captures occur within the swash zone. Infragravity waves propagating within the surf-zone facilitate additional capture events and therefore indirectly contribute to these large run-up instances. The magnitude of the bound infragravity wave associated with wave groups can be approximated using the crest-trough correlation, which captures the groupiness of the incoming wave field. The crest-trough correlation parameter was used as a proxy for infragravity energy and found to better predict run-up behaviour when included in an empirical parametrization with $\sqrt{HL}$.

Contents

List of Figures

Acknowledgements

I am deeply grateful for my supervisor Dr. Johannes Gemmrich, for his guidance and mentorship throughout my project. His unwavering support and encouragement was instrumental in completing this research and inspiring my passion for the field. Thank you for your patience, kindness, and wisdom.

I would also like to thank my supervisor Dr. Jody Klymak for his insightful comments and suggestions on my research. His expertise and profound understanding of physical oceanography has been crucial to the development of this thesis. Dr. Klymak's high standard of intellectual rigor and academic excellence is something I strive to emulate.

Thank you to Dr. Brad Buckham for bringing a valuable perspective to my research and for support with instrument deployment. This study would not have been possible without the support in conducting our field work, for this I would like to thank Liam McNeil and his team at Parks Canada.

I would also like to thank all my colleagues in the Ocean Physics group at UVic for the camaraderie, moral support, and thoughtful discussions. And a final acknowledgement to Leah Cicon, a brilliant researcher and dear friend who was there for me rain or shine to help with field work, provide encouragement, or just go for a bike ride.

This work was supported by the Search and Rescue - New Initiatives Fund (SAR-NIF) and Pacific Rim Ocean Data and Mobilization and Technology (PRODIGY).

Motivation

Wave hazards such as rip currents and extreme wave run-up pose a serious risk to people recreating in the surf-zone or on the beach. These hazards are particularly concerning in areas with energetic wave environments and high levels of tourism/recreation along the coastline, such as Vancouver Island's West coast. The study areas of this project include beaches within the Pacific Rim National Park and near Tofino, B.C. which are popular destinations for over half a million visitors that the region receives each year. This tourism prompts a need for local risk managers to be able to accurately assess and predict wave hazards in an effort to reduce injuries and fatalities on their beaches. People often walk within meters of the average run-up extent on the beach, not expecting the water to reach them. In the case that someone is knocked off their feet and pulled into the water, it can often be very difficult for them to get back to safety because their clothing is soaked and weighing them down. Identifying the driving factors behind wave hazards will improve the ability to accurately inform the public of the risk level posed by rip currents and extreme wave run-up on a day-to-day basis.

Studies on run-up have been conducted on natural beaches (Guza and Thornton, 1980, 1981, 1982; Stringari et al., 2019), in wave tanks (Tissier et al., 2015; De Bakker et al., 2016), and utilizing models (García-Medina et al., 2017; Fiedler et al., 2020). While there has been some success in predicting run-up behaviour in laboratory settings and with modelled simulations, these results are not easily translated to natural beaches. As long-term monitoring of beaches can be difficult to carry out, studies in the existing literature are on the order of days to week (Guza and Thornton, 1980, 1981, 1982; Stringari et al., 2019). These studies are useful, but generally limited in their application as they do not observe run-up over a variety of wave conditions.

This research will identify links between offshore conditions and onshore wave hazards. This can be used by risk managers, in conjunction with an improved model of the local wave field, to predict the relative risk to the public. Of interest to the broader scientific

community, this work provides a comprehensive case-study on wave transformation from deep water depths, to shallow water depths, to run-up on the beach.

Introduction

Previous characterizations of the run-up spectrum (Guza and Thornton, 1980, 1981, 1982) have shown a consistent shift to lower peak frequencies, with greater spectral transformation observed on highly dissipative beaches. Many in-situ studies of run-up on natural beaches are unable to adequately characterize the run-up spectrum because the length of the study and resulting time-series are not long enough for spectral analysis. This study is novel in that run-up is observed over multiple years, rather than on the order of hours or days as is most common in the field. The amount of run-up data obtained here allows for robust characterization of the run-up spectra across various sea-state conditions.

Where local hydrodynamic models or long-term observation of run-up are not feasible, empirical parametrizations are important in improving predictions of coastal flooding using regional and global models. Many of these parametrizations utilize $\sqrt{HL}$ (Hunt, 1959; Holman and Sallenger, 1985; Holman, 1986; Nielsen and Hanslow, 1991; Stockdon et al., 2006), which is derived from Hunt's (1959) formula and is dependent on both significant wave height and wave period, with L being deep water wavelength. Some of these parametrizations also utilize foreshore slope β (Hunt, 1959; Holman and Sallenger, 1985; Holman, 1986), to account for the differences in run-up behaviour between steeply sloping and highly dissipative beaches. While these various empirical formulations perform well within the conditions over which they were calibrated and validated on, they are prone to significant error when applied to a wider variety of beach and wave conditions (Power et al., 2019), making them unreliable for use in large-scale coastal flooding models. Infragravity waves and beach morphology have been identified as two key factors not accounted for in the commonly used parametrizations currently in use that could be contributing to their poor performance when applied more broadly (Dodet et al., 2019). In this thesis, the role of infragravity waves in determining run-up is explored using direct measurements, and then a practical proxy for infragravity energy is presented that could be included in empirical parametrizations to improve performance.

In this section, I will introduce the terms and concepts relevant to the study of nearshore

wave dynamics. I will also discuss the history of research in this field, with a focus on previous studies of wave run-up on natural beaches.

Definition of run-up

Run-up is driven by waves and is defined here as the maximum distance measured along the foreshore with respect to the local sea water level (Fig. 1).

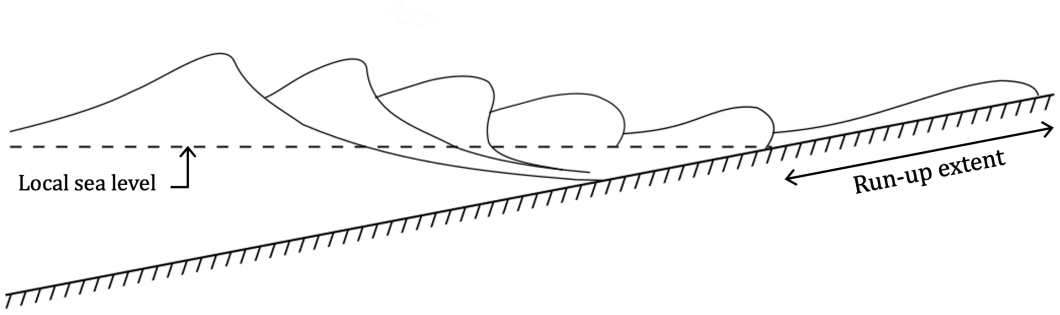

Figure 1: Diagram of run-up on a sloping beach. Adapted from Komar (1998).

Typically run-up is defined as the maximum vertical elevation of swash above local sea-level. This can be easily converted into the distance water extends up the foreshore (the definition of run-up used in this thesis) by dividing by the sine of the slope of the beach.

There are two components to runup: setup and swash. The process of waves breaking as they approach the beach gives rise to a momentum flux in the onshore direction, this is balanced by a pressure gradient that alters the mean sea level, called setup (Newell et al., 2005). Fluctuations around this heightened sea level mean determined by setup are what is defined as swash. Wave height, wave period and beach slope are all factors in run-up extent (Sorensen, 2006). The probability of extreme run-up occurrence is of particular interest due to the risk it poses to coastal infrastructure and people on the beach that may be caught off-guard.

Wave Breaking

When waves move from offshore into a shallow water environment, they begin to "feel" the sea-floor and undergo wave breaking as a result. When waves make contact with the bottom, in depths approximately half the given wavelength, they slow down. The wavelengths of the

incoming waves shorten as a result, leading to a steepening of the wave. Eventually the faster moving crest of the wave becomes unstable and breaks.

Based on particle motion at the crest, three breaker types are broadly recognized: spilling, plunging, and surging (Figure.2). While they are commonly discussed as distinct classifications, in reality these breakers all lie on a spectrum of wave breaking characteristics. The slope of the beach dictates the rate at which the wave slows, and thus its breaking behaviour. A gently sloping beach will yield a spilling breaker that dissipates its energy gradually across the surf zone. A steeper beach will generate a wave instability more abruptly and cause a plunging breaker where energy is dissipated rapidly near the initial break point. Surging breakers occur when the wave does not have enough time to steepen and break before reaching the shore, either due to a very steep slope or a long wave period. The result is some combination of energy dissipation at the beach-water interface and a reflection of the wave energy back offshore.

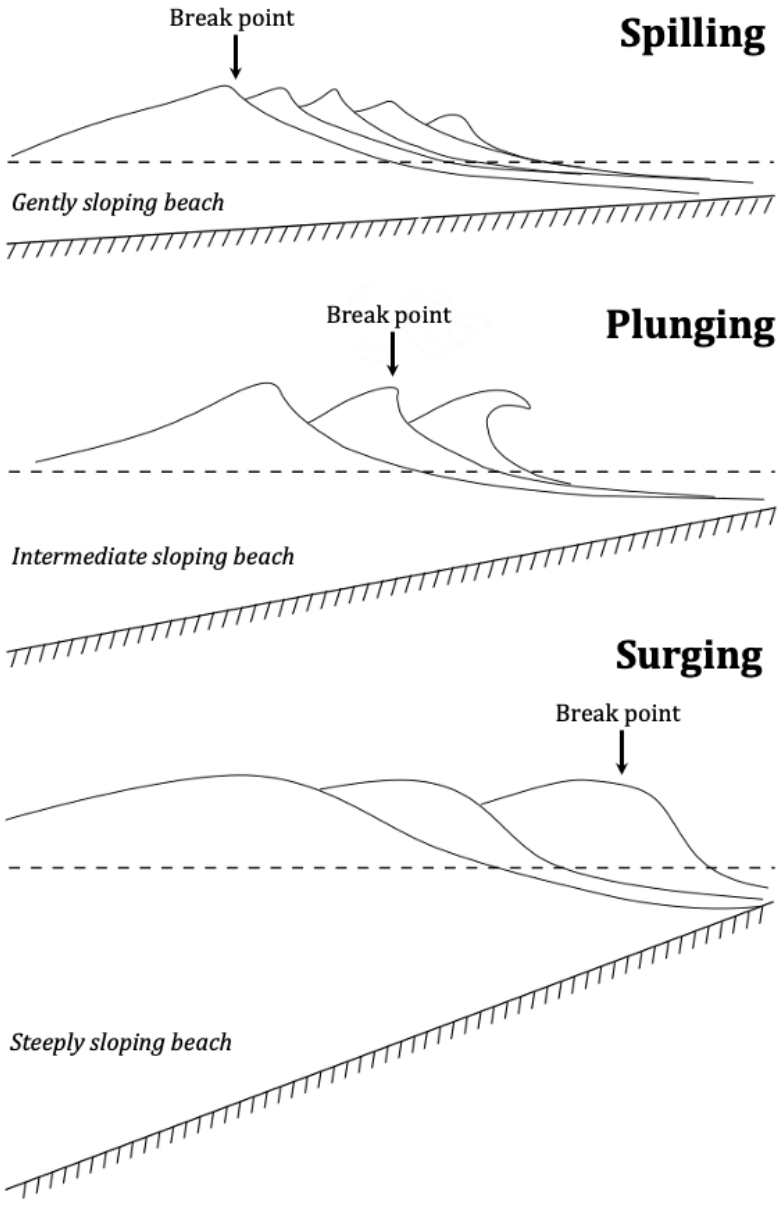

Figure 2: Three classifications of wave breakers. Adapted from Komar (1998).

The Iribarren number ξ is commonly used in parametrizations of wave breaking (Eqn. 1), where β is the slope, H is the wave height, and λ_0 is the deep water wavelength.

$$\xi = \frac{\beta}{\sqrt{H/\lambda_0}} \tag{1}$$

This parameter was found to be very useful in predicting wave breaking patterns by Battjes (1974). In these laboratory experiments conducted in wave tanks, spilling breakers occurred when $\xi < 0.4$, plunging breakers occurred when $0.4 < \xi < 2.0$, and when ξ exceeded 2.0 surging breakers were to be expected.

While there is a strong theoretical understanding of waves physics and wave characteristics can be reasonably predicted in laboratory experiments, natural beaches have many factors which cause wave behaviour to deviate from the expected regime. Weishar and Byrne (1979) conducted one of the first field studies to test the Iribarren number classifications on a natural beach and found it was an ineffective predictor. Laboratory studies predominantly look at monochromatic waves across a constant slope, whereas natural beaches have complex bathymetry and varied wave spectra shapes. This means that multiple breaker types can be occurring across a single field site; with bottom features such as sand bars playing a significant role in wave breaking, and instances where broken waves rebuild and break multiple times before reaching the shore.

Nearshore infragravity waves

Previous run-up observations show a strong infragravity signal in the resulting run-up spectrum (Guza and Thornton, 1982), with dominant periods between 30 seconds and 5 minutes, rather than the wind-wave frequencies typical offshore (Figure 3). As infragravity waves within the surf-zone have been shown to influence run-up behaviour (Tissier et al., 2015; García-Medina et al., 2017; Stringari and Power, 2020), the likely sources of infragravity waves entering the surf-zone and generated within the surf-zone are discussed below.

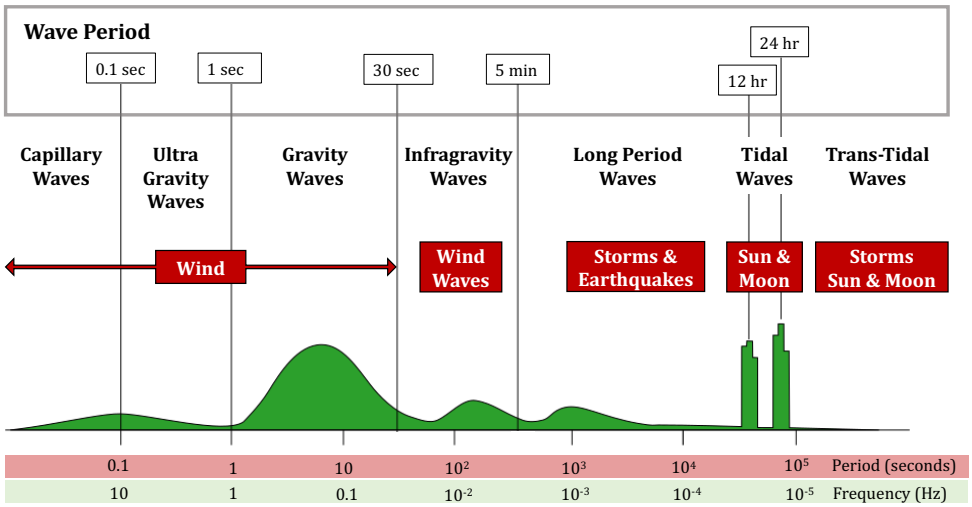

Figure 3: Ocean wave types classified according to frequency. Relative energy in wave spectrum illustrated by green curve. Red boxes contain the generating source for wave classifications. Adapted from (Ardhuin and Orfila, 2018).

There are two primary mechanisms for infragravity wave generation, one offshore and one in the shoaling zone, as well as smaller processes that can generate and amplify infragravity signals in the inner surf zone and swash zone. The first mechanism of infragravity wave generation is associated with wave groups that form from the superposition of wave trains with different frequencies (Figure 4). The larger waves in a group transport more momentum and depress the relative water depth, while this relative water depth is elevated under the smaller waves with less energy. This results in a bound infragravity wave with the same frequency as the wave group and a height around 1 cm. When the wave group enters shallow water, the bound infragravity wave is released from the wave group and propagates freely towards the shore with the same speed as individual wind-waves. While higher frequency sea-swell waves break and lose energy through dissipation in the surf zone, the associated infragravity wave can stay constant or even increase, becoming relatively more important in the spectrum as water depths decrease.

In-situ measurements show an increase in infragravity wave energy towards the shore that cannot be accounted for by the previous mechanism (Huntley and Bowen, 1973; Guza and Thornton, 1981). This is due to the presence of edge waves, infragravity waves that reflect off the beach but are then refracted and end up re-reflecting off the beach (Holman, 1983). In this way the infragravity waves are trapped, continually reflecting and refracting

as they propagate in the longshore direction.

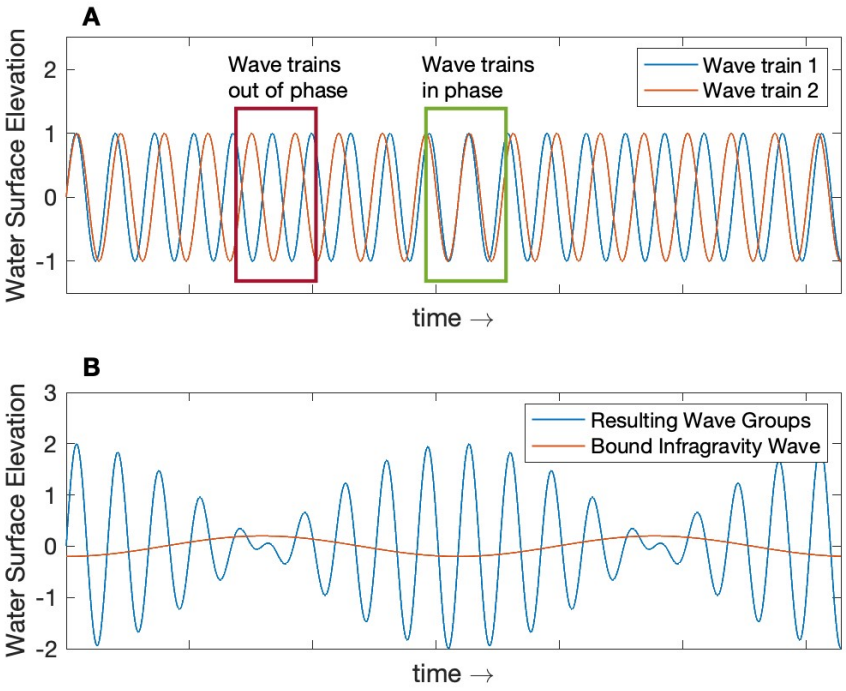

Figure 4: Upper plot shows the merging of two wave trains with different wavelengths. The resulting wave train has a group structure as seen in the lower plot.

Another source of infragravity waves arises from the time-variation of the radiation stress caused by larger waves in a group breaking further offshore than smaller waves (Symonds et al., 1982). Battjes et al. (2004) found that the previously discussed bound wave mechanism dominated over this breakpoint mechanism on dissipative beaches, so the latter is not considered relevant to this study.

In-situ studies of wave breaking and run-up

The first significant in situ study of wave run-up on beaches took place in 1977 (Guza and Thornton, 1980) and used voltage readings from dual-resistance wires along a transect to determine the interface between water and sand. This field campaign also utilized pressure sensors and current meters to study wave behaviour across the surf-zone as well as onshore, and yielded multiple publications (Guza and Thornton, 1980, 1981, 1982). Wave spectra were generated from the run-up timeseries to study the energy at various frequencies (f). While

a developed wave field has a spectral roll-off of f^{-4}, the swash spectrum was found to have a slope of f^{-3} (Guza and Thornton, 1982). This finding agrees with a previous laboratory study of swash (Webber and Bullock, 1968) which also showed a f^{-3} spectral roll-off. The second signifcant finding emphasized by Guza and Thornton (1982) is that unlike wind-waves, infra-gravity motions do not become saturated and consequently contribute significantly to swash oscillations at those low frequencies.

There were issues with the methodology of these early studies; the wires had to be monitored closely while data were recorded and were susceptible to interference from debris in the water, humans/dogs on the beach, and shifting sand (Guza and Thornton, 1980; Holman and Guza, 1984). This limited the duration of data collection and with improvements in camera technology, video recordings were adopted for monitoring run-up (Holman and Sallenger, 1985).

Holman and Sallenger (1985) utilized cameras to study wave run-up and set out to relate the Irribaren number, which had proven to be a useful parameter for run-up in laboratory experiments, to field observations. The findings were that for low Irribaren numbers, the wind-wave frequencies of the swash spectra become saturated and infragravity motions are dominant. At high Irribaren numbers, proposed as anything above 1.75, these saturation effects were absent.

Based on the commonly used definition of vertical run-up, significant swash run-up (R_S) is defined as the maximum vertical elevation of run-up above local sea-level. Guza and Thornton (1982) proposed that R_S was entirely dependant on the offshore wave height (H_{inf}):

$$R_S = 0.7H_{\text{inf}} \tag{2}$$

Holman (1986) argued against a constant ratio between run-up and wave height as proposed by (Guza and Thornton, 1982), arguing instead that there is a dependence on the Iribarren number. Holman (1986) derived a parametrization for extreme run-up (eqn. 3), seeking to predict the 2% exceedence of run-up elevations ($R_{2\%}$).

$$\frac{R_{2\%}}{H_{\text{inf}}} = 0.45\xi_{\text{inf}} \tag{3}$$

The parameter $\sqrt{HL}$ can be derived from the above equation and has been shown to be linearly related to run-up (Hunt, 1959; Stockdon et al., 2006; Li et al., 2022).

Nielsen and Hanslow (1991) studied wave run-up on a variety of beaches and found that

for dissipative beaches (defined as beach slopes less than approximately 0.10), run-up were independent of beach slope or incoming wavelength. This suggests that a relationship similar to that of eqn. 2 may be more appropriate for gently sloping beaches.

Bore-bore capture (BBC)

Bore-bore capture is the process by which a bore propagating towards the beach catches up with the preceding bore (Figure 5). Local water depth determines a fully developed bore's velocity (Bergsma et al., 2019). Water depth is dependent on the size of a given bore, the set-up from preceding bores, and infragravity waves. These factors lead to variable water depths that allow for the merging of bores in the surf and swash zones. Processes that affect sea-swell waves also determine the likelihood of bore-bore capture occurring. Frequency dispersion in deep water causes shorter period waves to have a lower velocity than long period waves, and amplitude dispersion increases the speed of high waves relative to small waves (Svendsen, 2006). These effects on waves before they become fully developed bores can lead to more instances of bore-bore capture.

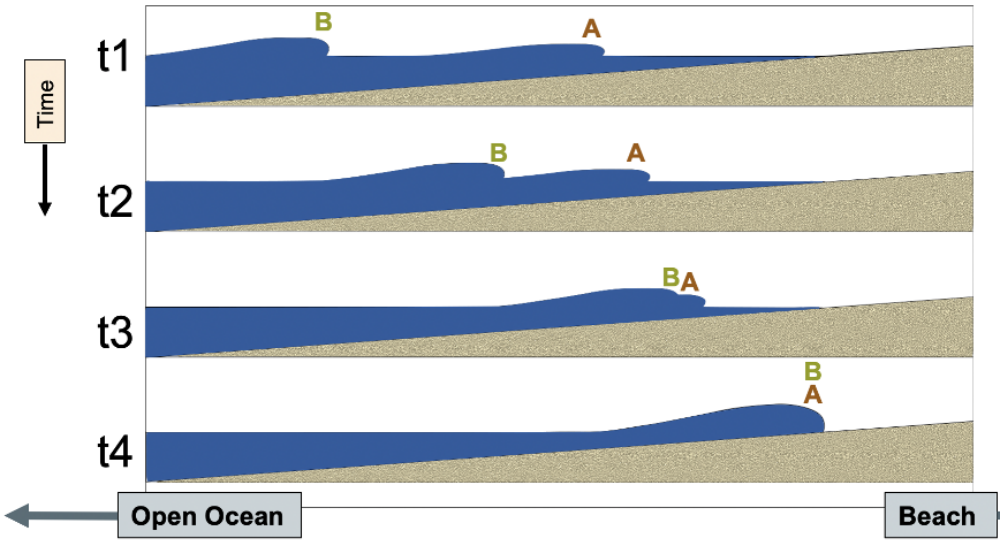

Figure 5: Diagram showing how two bores propagating beachward can merge into one larger bore before running up the foreshore.

Bore-bore capture has been increasingly studied in recent years to determine its role in generating extreme run-up events (Tissier et al., 2015; García-Medina et al., 2017; Stringari and Power, 2020). Senechal et al. (2011) showed that the merging of bores could contribute

to the shift of energy from the sea-swell frequency band to the dominance of the infragravity frequency band observed in run-up. As bore merging contaminates the spectrum by producing a signal in the same frequency band as infragravity waves, it can be difficult to quantify the relevant contributions of these two factors. As infragravity waves modulate water depth, and therefore the celerity of shoreline propogating waves and bores, they can also contribute to the occurrence of bore-bore capture. Tissier et al. (2015) used a non-hydrostatic wave-flow model to show this, finding that bore merging was strongly correlated to the ratio between infragravity wave height and water depth. García-Medina et al. (2017) modelled extreme run-up events and found that the largest instances were associated with bore-bore capture. This study (García-Medina et al., 2017) found that while amplitude dispersion drives bore-bore capture in the outer surf zone, interactions with infragravity waves becomes a dominant process for generation of bore-bore capture events in the inner surf zone.

Stringari and Power (2020) studied run-up on natural beaches where bore-bore capture was observed, finding a 40% chance that an incoming bore would be captured in either the surf or swash zone. Extreme run-up events were driven by these previously captured bores in 97% of cases, underscoring the importance of this mechanism in generating the largest observed run-up. The likelihood of capture was discovered to increase towards the shoreline, with 46% of bore-bore capture events occurring in the swash zone. These events that occur near the interface between the ocean and beach are referred to as instantaneous bore-bore capture, and were more likely to result in an extreme run-up event than bores that merged in deeper water (Stringari and Power, 2020).

Methods

Observations of run-up on a highly dissipative sand beach were collected using video imagery recorded over a period of 2 years. These run-up data are correlated to measurements from multiple wave buoys and a pressure sensor to better understand the processes determining run-up behaviour and to find methods to improve run-up paramaterizations commonly utilized in large-scale models.

Regional setting of field site

Video monitoring of wave run-up occurred on Wickanninish Beach in the Pacific Rim National Park, a location where extreme run-up had been identified as a risk to beach-goers by Parks Canada officials. Wickanninish Beach is located at the South end of Long Beach, a southwest facing 16 kilometer sandy beach between the towns of Tofino and Ucluelet on Vancouver Island's West Coast (Figure 6).

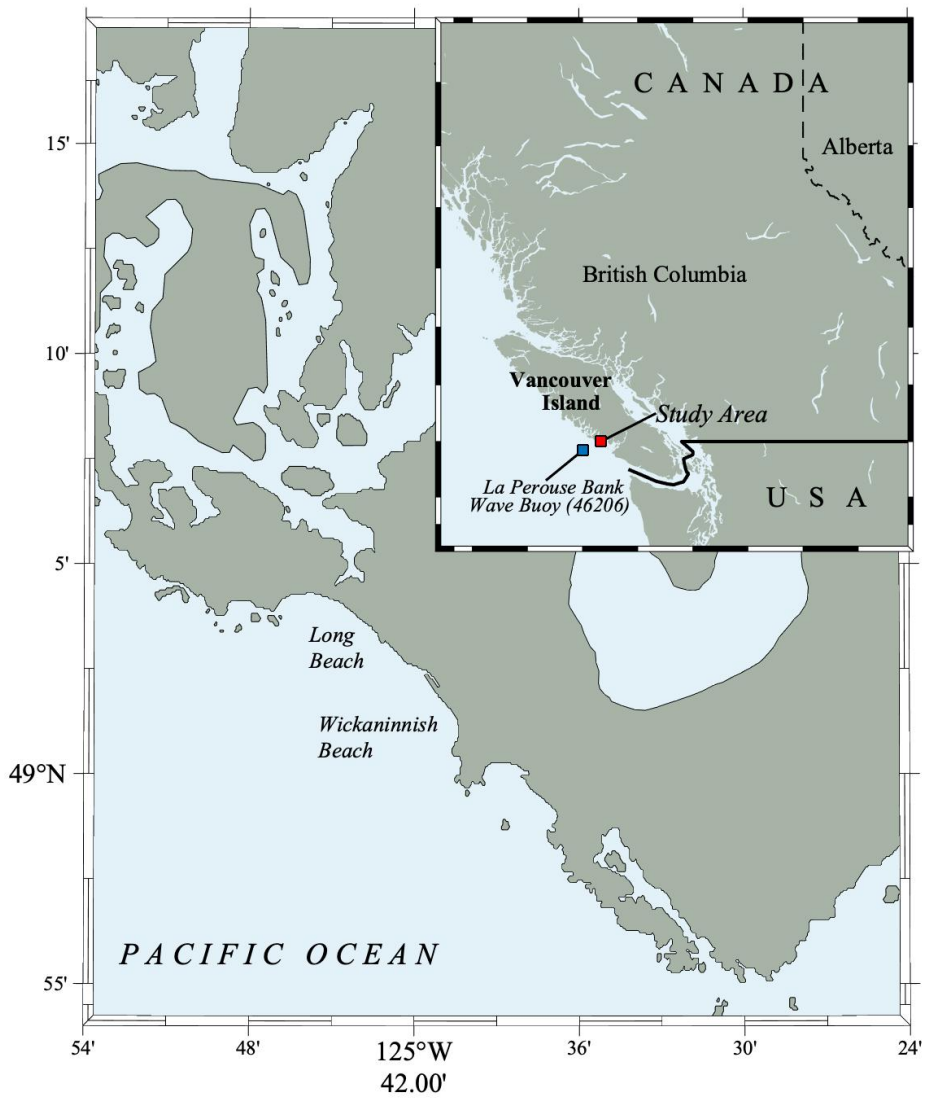

Figure 6: Map of study area showing the location of Wickanninish beach within the Pacific Rim National Park on western Vancouver Island, British Columbia, Canada.

Pacific Rim Park is exposed to the open ocean, where the incoming wave field is largely the result of distant storms happening offshore rather than local winds. The direction of incoming waves differs seasonally, with west and southwest swell being dominant in the winter, and west and northwest originating waves becoming more common in the summer ((Thomson, 1981)). The duration and strength of winds associated with these differing sources, as well as the fetch, result in the observed seasonality of waves on B.C.'s West

Coast. From June to August, the sea state is typically calm with significant wave heights around 1-2m (Figure 7). This abruptly changes in October and continues throughout the winter storm season where significant wave heights are relatively high, often exceeding 5m. This seasonality is also reflected in the peak wave period, when distant storms from the South dominate in the winter the extended fetch enables a stronger lower frequency swell to form.

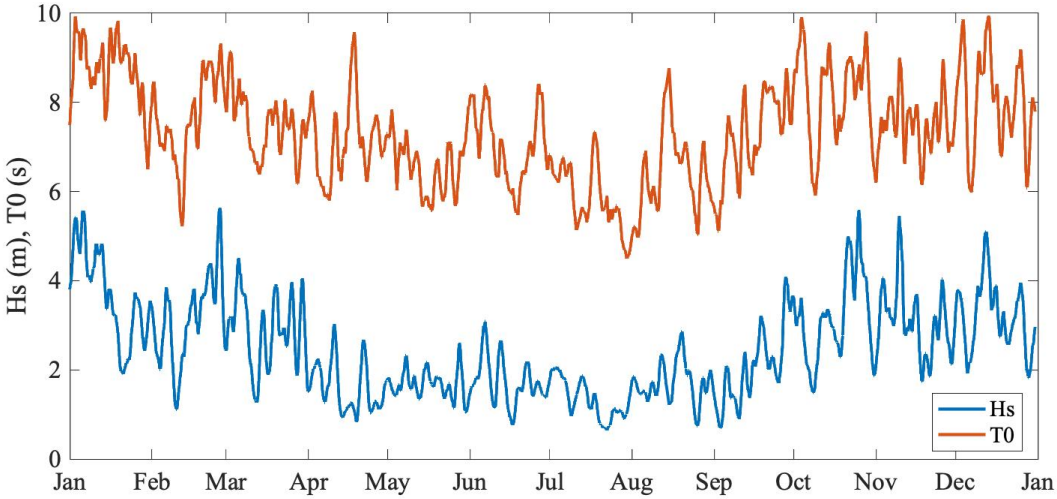

Figure 7: Two day average of significant wave height and peak period from LaPerouse Bank buoy (46206) for the year 2021.

Beach characteristics

Figure 8: Photo of beach taken from Kwisitis Visitor Centre facing northwest.

The run-up study area is a gently sloping beach with fine grained sand (Beaugrand, 2010). Figure 8 shows the view of Wickanninish Beach from the Kwisitis Visitor Centre (KVC), with the study site being the area in the foreground. Two surveys of the beach slope were conducted over the course of the study, starting at the logs at the edge of the beach and extending down to the water line (Figure 9). These surveys attempted to capture any morphological changes due to the wave environment in the months prior. The November survey shows the beach slope following smaller wave activity over the preceding boreal summer months. The second survey aimed to capture a "winter beach" driven by a more energetic wave field over the boreal winter; although June is later than ideal, evidence of sand transport between the two seasons would likely still be reflected in these data.

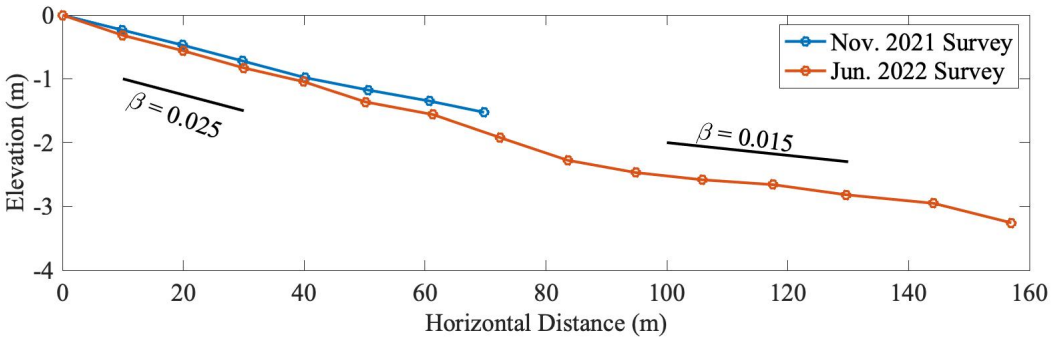

Figure 9: Slope of field site measured from position on the beach adjacent to the Wickanninish entrance path. Both surveys were conducted using a Spectra Precision Focus 6 Total Station. November 2021 survey took place during a neap tide, thereby limiting the length of the transect.

This region has a tidal range up to four meters, causing the location of the water line along the beach to vary by over 200 meters. In both surveys, the landward end of the swash zone (first 60 meters of the transect) is found to have a slope of approximately 0.025. In the June 2022 survey, the slope between 100 and 140 meters from the logs is even more gradual at approximately 0.015.

A hydrographic survey of Wickanninish bay was also conducted in July 2020 (Figure 10). The slope between the two points in the Figure 10, representative of the surf zone, was found to be 0.0087. This value is consistent with the slopes found from the total station surveys of the swash zone.

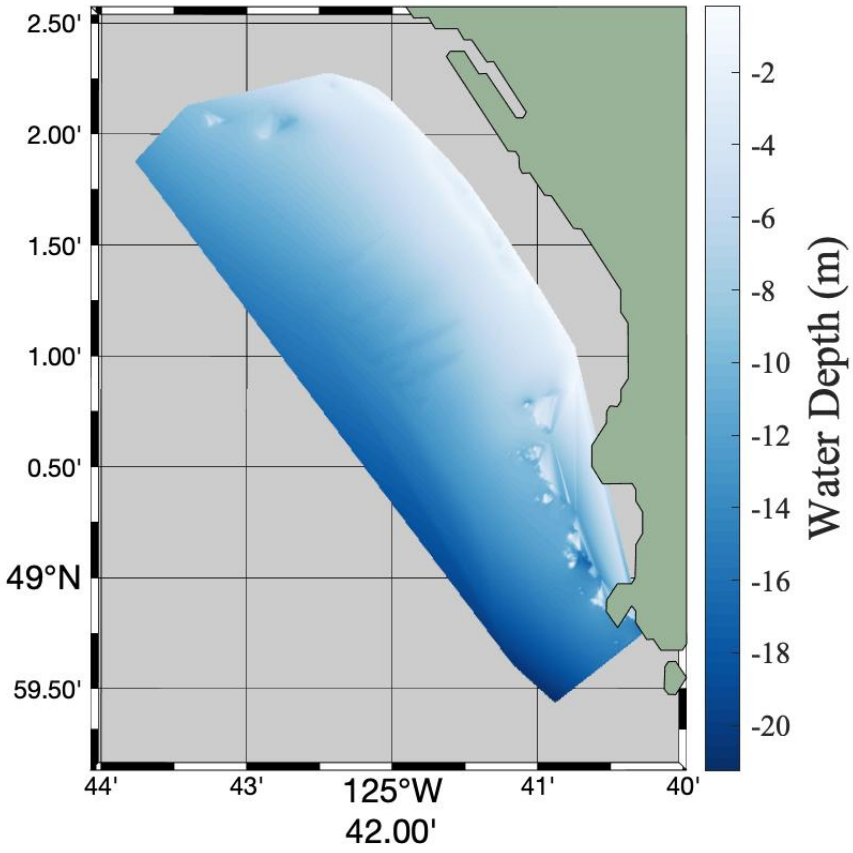

Figure 10: Bathymetry from a survey conducted by the Canadian Hydrographic Service on July 24-26 2020.

In-situ data

Data were utilized from offshore wave sensors in the analysis of the run-up timeseries. A TriAXYS wave buoy was deployed in approximately 20 meters water depth off of Wickaninish beach from the start of the study in November 2019 until the following summer. To measure waves immediately outside the surf zone, a Spotter (SOFAR Ocean) wave buoy was deployed in approximately 8m water depth for three weeks in October 2021 along with a pressure sensor (RBRsolo3 D). The Spotter buoy was redeployed in November 2021 in the same location. A summary of times of data collection for each source is shown below in Figure 11.

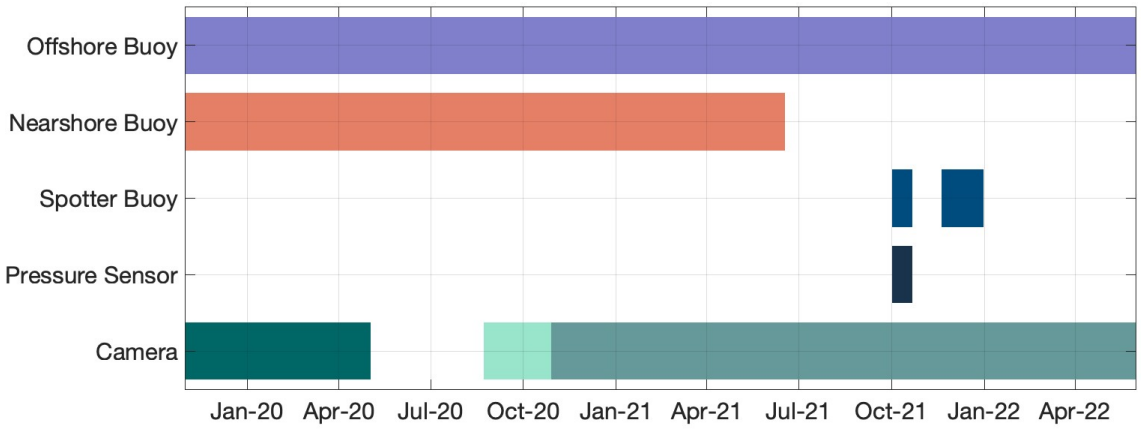

Figure 11: Data coverage from various instruments utilized in study.

Camera Data

Video footage of the beach was obtained using cameras mounted on the side of the Kwisitis Visitor Centre (KVC) facing northwest over Wickanninish beach. A visible light camera (Prosilica GC1350) recorded between 8 to 16 hours of the day, depending on the time of year. The characteristics of run-up are of particular interest during the winter storm season, during which the visible camera is only recording for approximately one third of the day. To overcome this, an infra-red (IR) camera (FLIR A65) was also installed and recorded near continuously year-round for the duration of the study at 5 frames per second. In addition to the lack of temporal continuity with the visible camera, the presence of people in the frame of view and sun glint on breakers made processing the visible light footage difficult, therefore only data from the IR camera is utilized in this analysis.

The Kwisitis Visitor Centre was under construction for the duration of the study, and the cameras were taken down from their initial position (position 1) in the spring of 2020. They were set up in a temporary location over the summer (position 2) with a limited field of view, and then reinstalled at the initial location with a similar field of view in the fall of 2020 where they remained for the rest of the experiment. Additional discontinuities in the recording were due to power outages at the centre.

Extracting a Timeseries

Due to the large amount of data collected, automating the extraction of the timeseries as much as possible was necessary. An algorithm was utilized that can be applied to any video

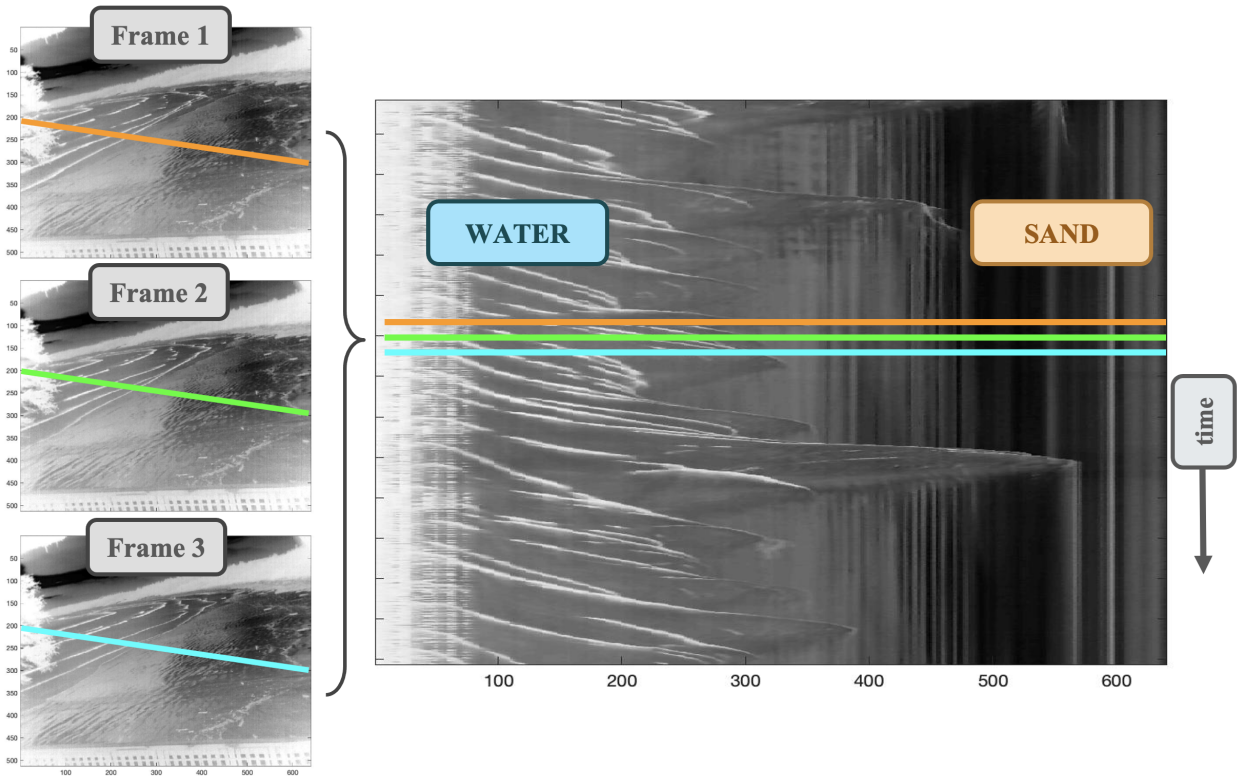

Figure 12: Example showing how a timestack is generated from video footage.

footage, independent of the location. To extract a timeseries of run-up, transects of the beach were taken from the video data to generate a timestack (Figure 12). This produces a matrix where one axis is pixel intensity, showing the interface between water and sand along that transect, and the other axis is time. From here I am able to apply a thresholding method to trace out the run-up timeseries.

In order to eliminate signals from stationary items that may be in the field of view (logs, seaweed, etc.), the difference between timestacks over a period of two seconds is taken. The image is then binarized using a variable threshold that is optimized for each ten minute timestack. The goal is to maximize the number points along the interface which a timeseries can be fit to, without introducing too much noise into the timestack and obscuring the signal of the run-up. The threshold value also acts as a proxy for the quality of the timestack, and poor quality data are easily excluded from future analyses by filtering out parts of the timeseries where a low threshold value was required.

The most difficult variable to deal with in this post-processing is the presence of humans and animals, which are picked up strongly by the infrared camera. These signals are not

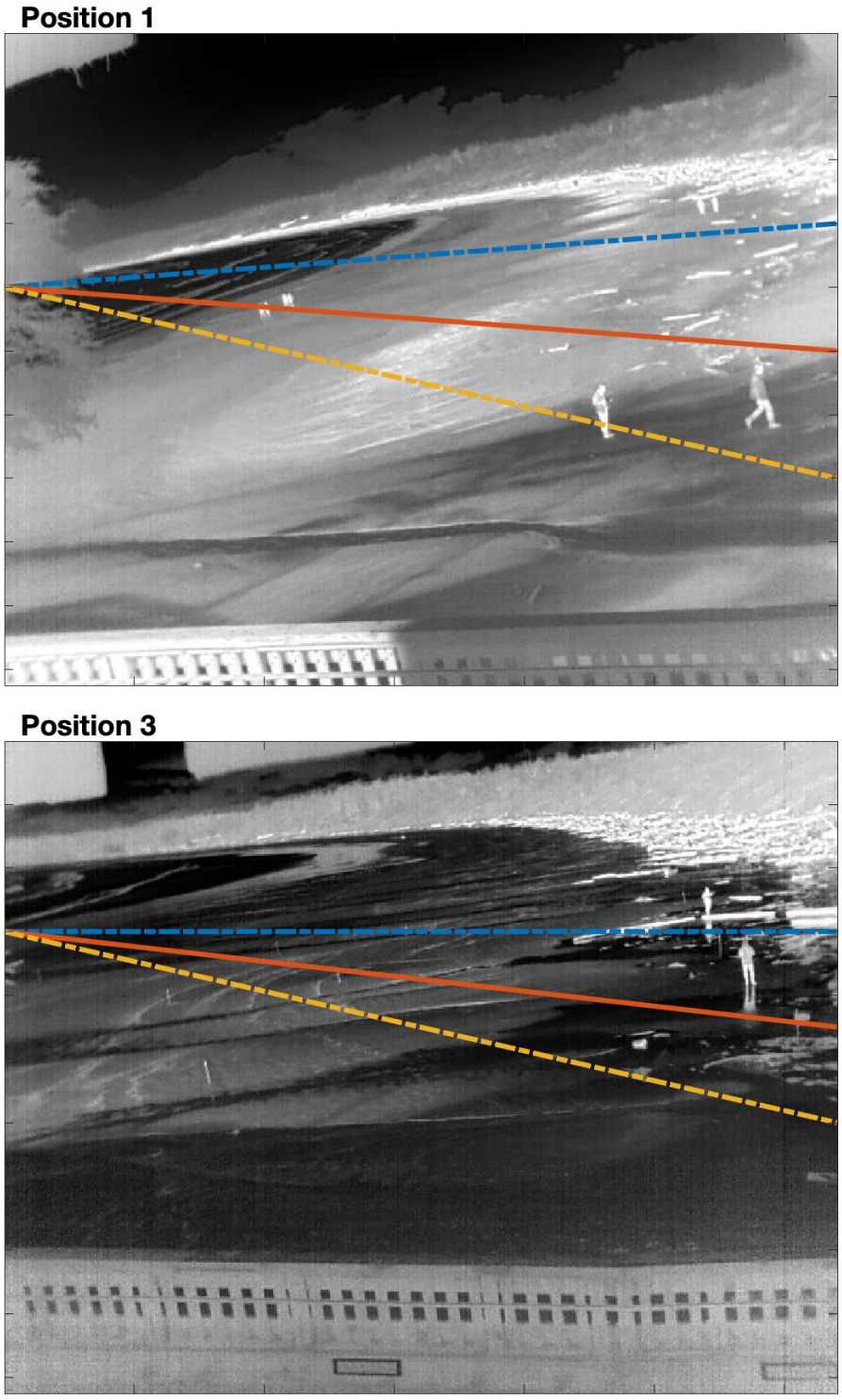

Figure 13: Frame from camera at each position. Position 1 (top) was used from November 2019 to April 2020, position 3 (bottom) was used from October 2020 to May 2022. Three lines on each frame show the cross sections used, the red (center) line is used for the data analysis with adjacent transects used for automated cross referencing of extremes.

eliminated in previous steps since they are nearly always in motion, and surfers entering and exiting the water along a chosen transect can even mimic the shape of a swash motion in the timestack (Figure 14). Due to the nature of how animals and people interact with the water's edge, by either walking along the beach or entering/exiting the ocean, these erroneous signals commonly show up as extreme swash events.

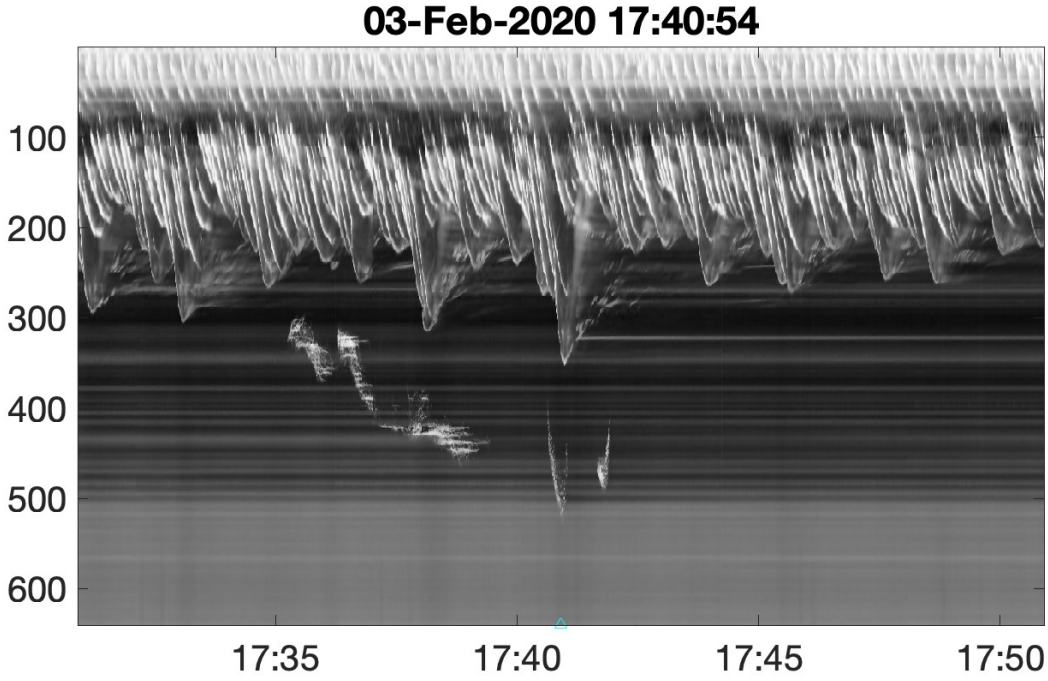

Figure 14: Example showing how a human may show up in the timestack.

These human obstructions pose a problem because extreme swash events are inherently infrequent, so it does not take many of these occurrences to significantly skew the overall statistics. To address this, timestacks are taken from 3 different transects and any extreme events from the primary timeseries are removed unless the feature is also present in the adjacent timestack (Figure 13). The assumption here is that the cross sections are close enough together that the same swash motions would be measured in each, but far enough apart that a human present in one transect would not be tall enough to interfere with the adjacent transect at the same time. This cross-checking method is effective in filtering out erroneous extremes, but is only applied to outliers above a certain threshold and ignores human signals in the timeseries that are not registered as extremes. As these events are rare relative to the total number of swash motions (most of which are not extreme), these erroneous points (from humans, dogs, etc.) in the timeseries for average swash signals can

be ignored.

Once the raw timeseries of the interface between the water and the beach along the transect is generated from the timestack, it is transformed from pixels to real-world units of measurement. To achieve this we used wooden stakes to create a grid on the sand surrounding the transect used for the timestacks, these stakes are seen in Figure 8. The base of the stakes are manually selected from the IR camera frame and assigned real world coordinates. This method assumes a planar beach, which is a reasonable assumption given the profiles obtained from both surveys conducted (see Figure 9). The transformation of the raw run-up timeseries to the georeferenced and despiked run-up timeseries is seen in Figure 15.

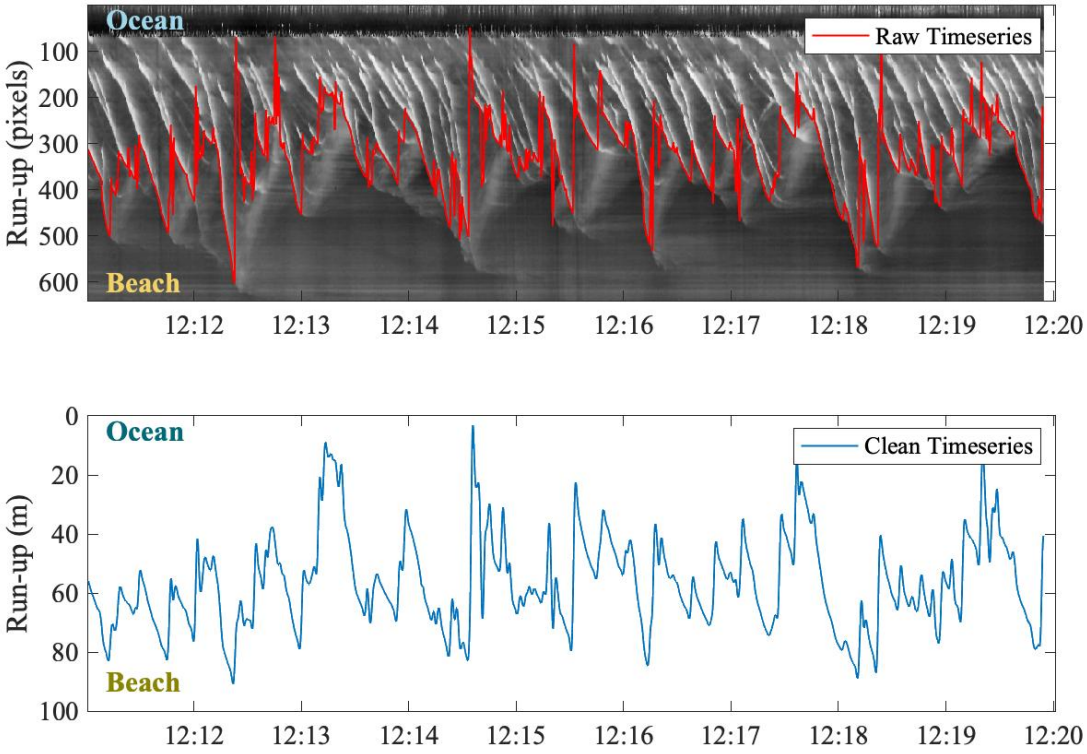

Figure 15: Top figure shows timestack from January 14, 2020 with the initial timeseries in red. Bottom figure shows the timeseries cleaned and adjusted to units of meters.

To study the maximum extent of each swash excursion, the local peaks are extracted from the clean timeseries. To normalize the swash extent, the distance is measured from a 20 minute running average of the 5^{th} percentile of the timeseries. A primary motivation of

this study is to understand wave run-up for the purpose of improving public safety. For this reason, the horizontal measure of run-up is preferred as this is how run-up is perceived by beach goers. Figure 16 shows how the swash maxima are flagged on the run-up timeseries. Measuring from this 'baseline' of swash removes slow changes in local sea level from tides, storm surge, and wave set-up.

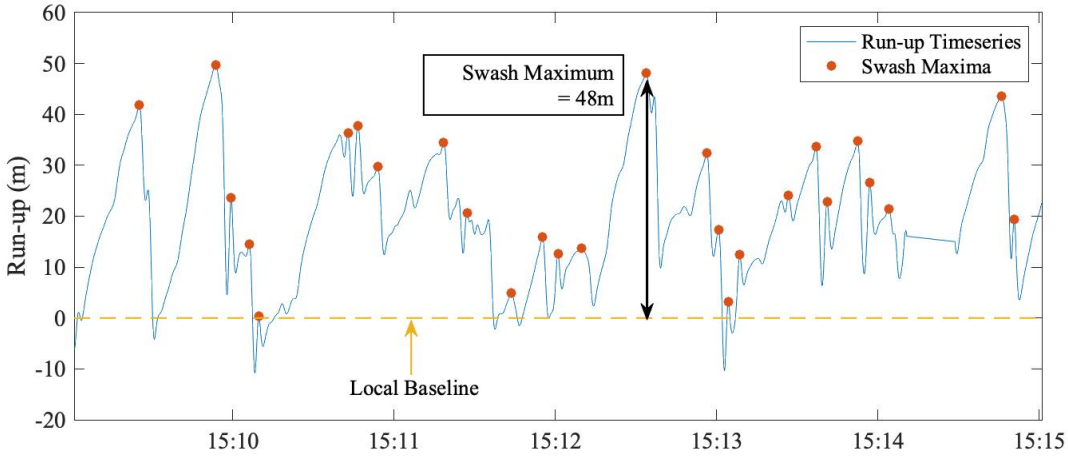

Figure 16: Example of how swash maxima are flagged from the run-up timeseries from a day in February 2020.

Justifying different camera positions

Due to construction on the KVC, the cameras had to be taken down six months into the project and were briefly installed over the summer to a position with a limited view of the beach. They were able to be placed back in the first location in the fall with the same field of view. A recalibration of distance using stakes on the beach was done for each position. Figure 17 shows the distribution of swash maxima between the two locations. As the distributions are similar, we assume there is no bias in the data between the two locations.

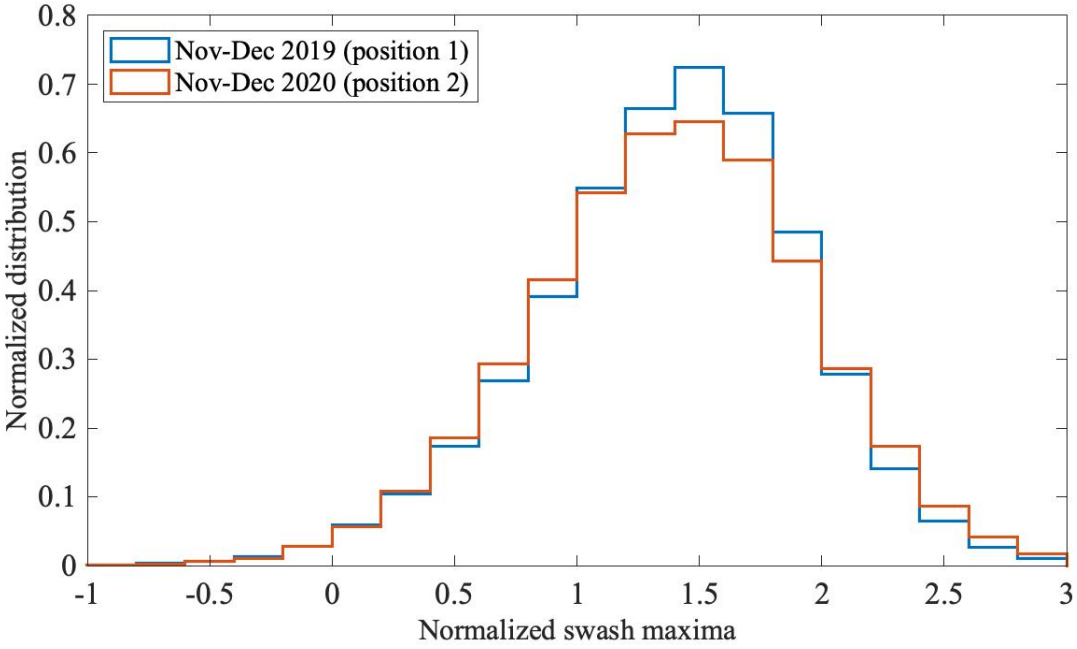

Figure 17: Comparison of run-up distribution from two different camera locations.

Data Analysis Outline

The run-up timeseries is studied using spectral analysis techniques and results are compared to spectral characteristics of the incoming wave field. All swash maxima are studied for correlations with the incoming wave field, with the extreme events taken from the tail end of this distribution.

Results

Run-up Distribution

The distribution of swash maxima is shown in Figure 18 and is fit with a Rayleigh distribution, which is the characteristic distribution of peak wave heights in a developed wave field.

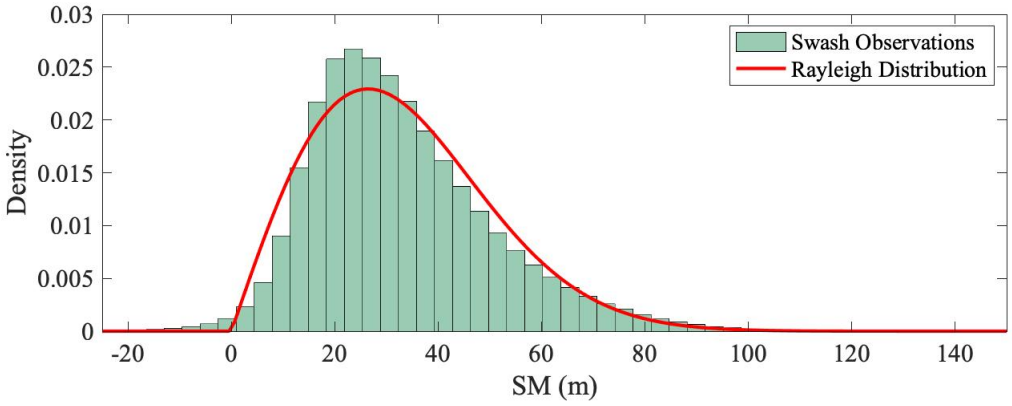

Figure 18: Histogram of all swash maxima measured from the 5^{th} percentile of run-up timeseries with Rayleigh distribution fit.

The Rayleigh distribution underestimates the frequency of mean swash maximas (15m to 45m), but does a good job of estimating the positive tail of swash maxima. Hughes et al. (2010) looked at the probability distributions for swash using field observations and found similar deviations from this theoretical PDF.

Spectral Shift

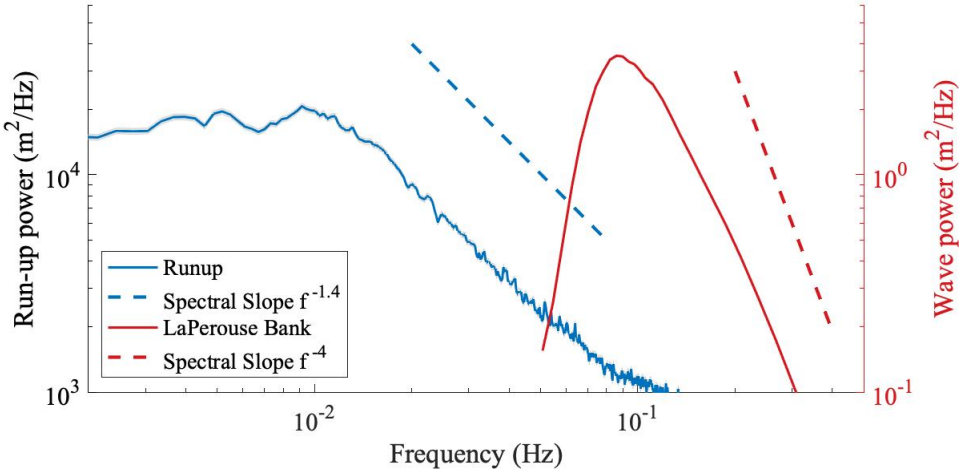

Figure 19: Spectrum from run-up timeseries (blue, left axis) compared to wave spectrum from wave buoy at La Perouse Bank (red, right axis).

Ocean wave spectra typically peak at around 10^{-1} Hz, corresponding to a wave period of 10 seconds. Spectra of fully developed wave fields also have a characteristic frequency dependence (roll off slope) of f^{-4} (Huntley et al., 1977). Swash spectra differ in that they have a lower peak frequency and a lower frequency dependence (Guza and Thornton, 1982). Figure 19 shows the spectra of run-up and the corresponding offshore waves. Wave buoys are unable to resolve low frequencies, so the range of the LaPerouse Bank spectrum is limited to between 0.05 Hz and 0.4 Hz. The swash spectrum peak is around 0.01 Hz and has a frequency dependence of approximately $f^{-1.4}$. While the spectral transformation is consistent with previous studies of run-up spectra, the findings presented here are more extreme than previously observed. Guza and Thornton (1982) finds spectral peaks between 0.02 Hz and 0.04 Hz and a spectral roll off of f^{-3}. It is often suggested (Guza and Thornton, 1982; García-Medina et al., 2017) that the transformation of the spectrum is dependant on beach slope, which could explain the shape of the swash spectra seen here. Given that the study site has a lower slope than previous in-situ studies, the resulting spectra is expected to have a higher degree of transformation. It is also likely that this part of the spectrum is impacted by the method of obtaining the run-up timeseries from the video footage. The thresholding technique utilized in this study detects the turbulent edge of the bore on the beach, which is stronger during uprush than downrush. For this reason, the timeseries tends

to track the advancing bore to the maximum extent of its excursion and then jumps down to the next bore advancing up the beach. This results in a saw-tooth pattern in the timeseries, leading to high frequency noise distributed across the shorter periods of the wave spectrum and distorting the slope dependence calculated here.

The peak frequency observed in swash spectra lies in the infragravity (IG) range, showing a clear shift in dominant energy from short wave (SW) to IG frequencies. We cannot determine from our measurements the absolute change in energy across the surf zone, so it is unknown whether IG energy actually increases or if SW frequencies are just dissipating at a faster rate.

Run-up variability vs. sea-state

Using the method previously explained for obtaining swash maxima data (see Figure 16), we relate run-up extent to sea-state variables to study how wave conditions influence run-up behaviour. Figure 20 shows the relation between run-up and the corresponding significant wave height (Hs) and dominant period (T0) from an offshore buoy. SM_{75} is 75^{th} percentile of swash maxima calculated over a 20 minute window. This gives a measure of "significant run-up extent" and was chosen to maximize the number of points obtained from the data. A higher percentile was not chosen as this could introduce error when applied across such a large data set where every swash maxima cannot be visually validated. The sea-state variables were calculated according the equations below, where m_0 and m_1 are the zeroth and first moment of the wave spectrum, respectively.

$$m_n(f) = \int_0^\infty f^n S(f) df \tag{4}$$

$$Hs = 4 \cdot \sqrt{m_0} \tag{5}$$

$$T0 = \frac{m_0}{m_1} \tag{6}$$

Run-up maxima demonstrates a positive correlation to significant wave height. Since these maxima are measured from the local 5^{th} percentile of the run-up timeseries, excursions do not include heightened water levels from storm surge and wave set-up. There is a similar trend with T0, wherein high periods observed offshore result in greater run-up excursions onshore. Another notable feature represented by these binned data is that the negative skewness also decreases with both Hs and T0. This shows that swash excursions above the

median have more variability (more relatively large instances) as Hs and T0 increase. These data show that both run-up distance and run-up variablity are positively correlated to the energy of the incoming wave field.

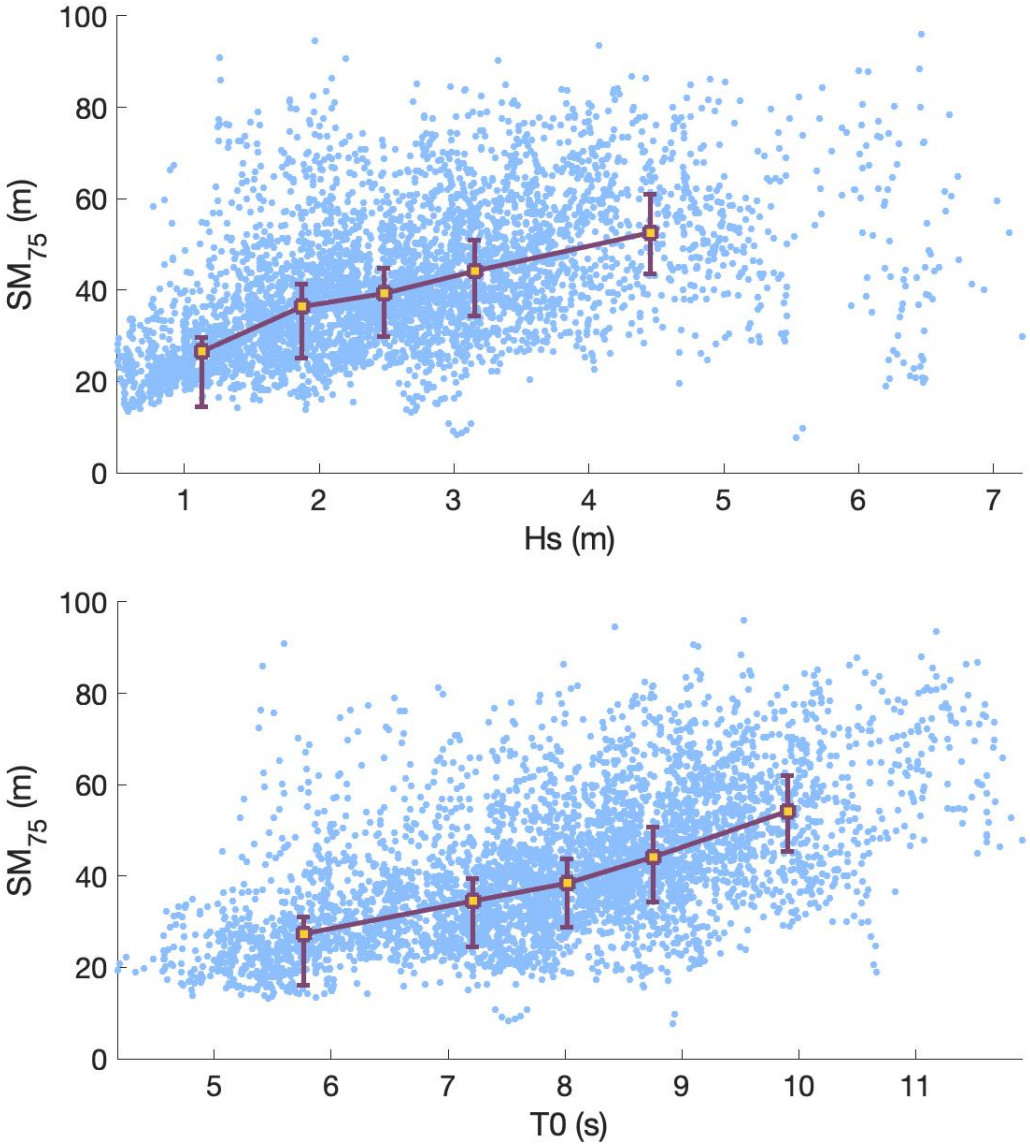

Figure 20: Binned run-up maxima plotted against significant wave height (top) and peak period (bottom) calculated from offshore La Perouse Bank wave buoy (46206). Blue dots are the 75^{th} percentile of swash maxima over 20 minute windows. Five equal-weight bins show the trend of these swash data. The yellow dot is the median swash excursion, and the vertical bars show standard deviation for the swash.

The parameter $\sqrt{HL}$ has been shown to relate to wave run-up (Stockdon et al., 2006)

and is commonly used in formulas to predict run-up maxima. Using this parameter (Figure 21) shows a strong linear trend with SM_{75}, and negative skewness at low values with the distribution moving to approximately zero skewness at the highest $\sqrt{HL}$ bin.

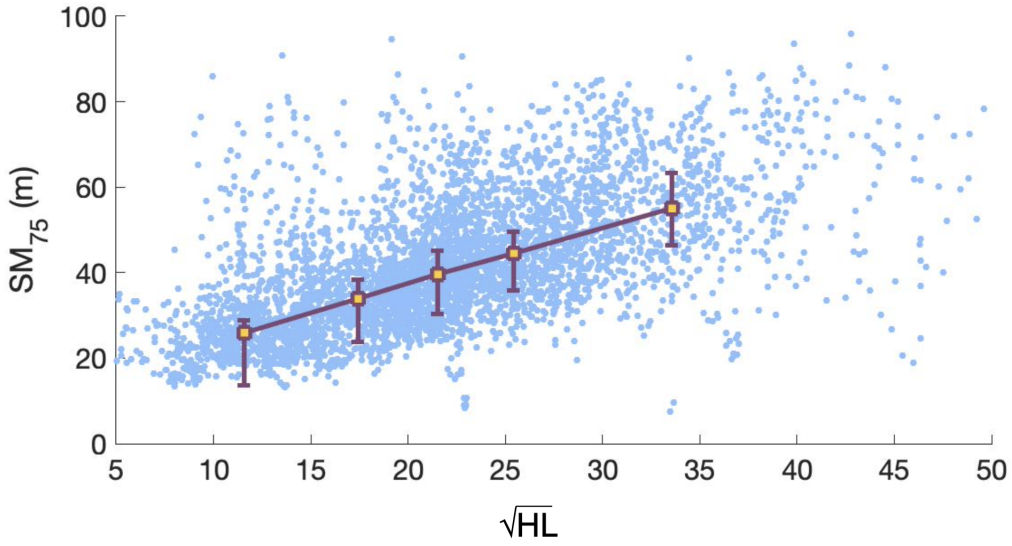

Figure 21: Binned run-up maxima plotted against parameter $\sqrt{HL}$ calculated from offshore La Perouse Bank wave buoy (46206). Blue dots are the 75^{th} percentile of swash maxima over 20 minute windows. Five equal-weight bins show the trend of these swash data. The yellow dot is the median swash excursion, and the vertical bars show standard deviation for the swash.

Seasonality

Seasonal differences in run-up behaviour arise due to shifting beach morphology, differences in magnitude and frequency of energetic wave conditions, and changes in the dominant direction of incoming waves. In looking at the distribution of swash maxima during different times of the year, we determine that changes in wave energy are driving the majority of observed seasonality in run-up. Swash maxima are the largest and most variable in December and January (Figure 22), and smaller and less variable in the summer.

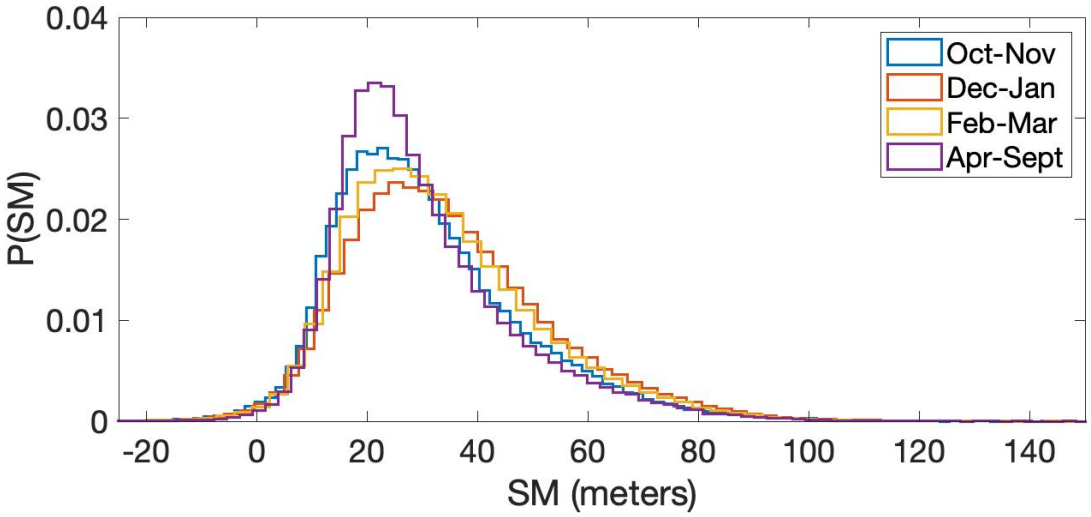

Figure 22: Seasonally binned distribution of run-up maxima.

The seasonal differences in runup distribution are consistent with those observed when swash maxima are binned by significant wave height and dominant wave period (Figure 23). Swash maxima are more widely distributed when sea states are energetic, which is more common during the winter months. When significant wave height and wave period are smaller, swash maxima are typically lower and there are fewer instances of runup extending significantly further than the mean. This suggests that seasonal differences in average runup behaviour are primarily the result of changes in energy of the incoming wave field. Therefore the distribution of swash can be reasonably predicted using only the sea-state variables, regardless of the season.

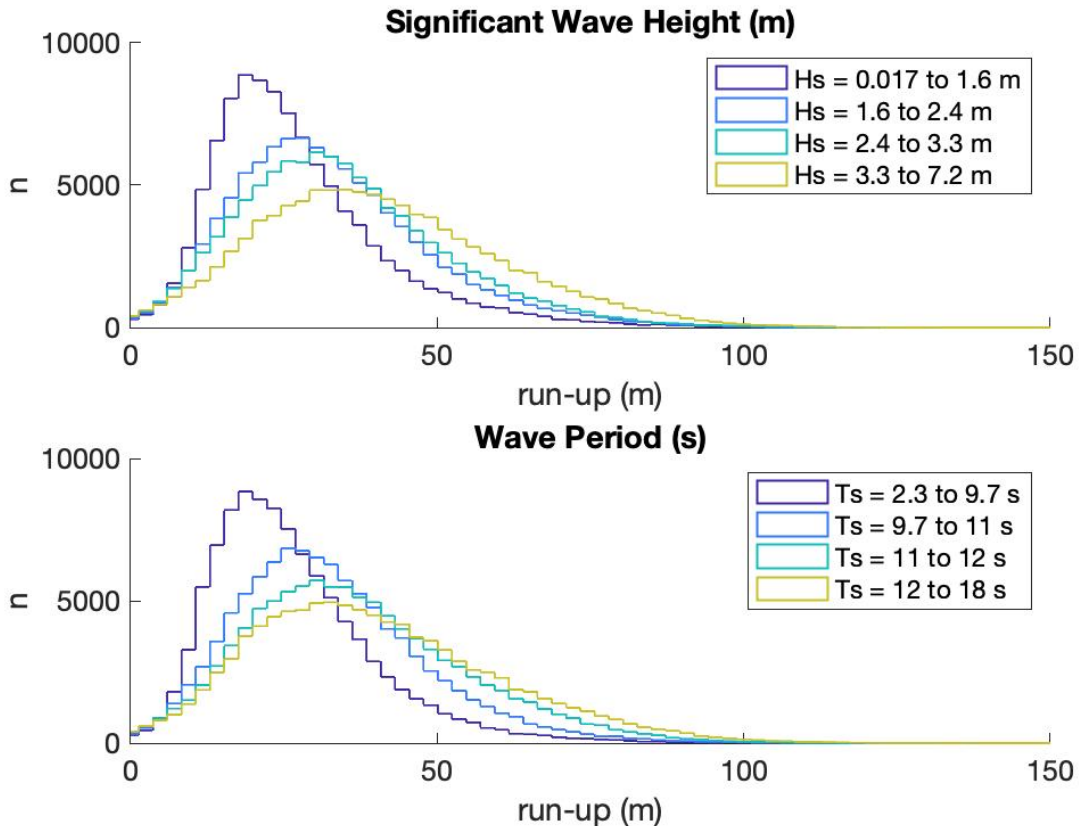

Figure 23: Histograms of swash maxima showing how the shape of the distribution changes with sea-state variables.

Seasonal changes in the swash distribution may be expected due to significant changes in the beach morphology throughout the year. To investigate this, swash maxima corresponding to sea-states between 2-3.5 meters and wave periods of 8-10 seconds were selected from the start of the winter storm season and the end of the winter storm season for comparison. If changes in the beach slope were significantly impacting swash behaviour, then we would expect to see different swash behaviour under similar sea-states between the two time periods. Figure 24 shows a scatter plot (top figure) and distribution (bottom figure) of SM_{75} for the two time periods November to December and February to March. As there are no obvious differences in the behaviour between the two subsets of data, it can be assumed that the effect of seasonal changes in beach morphology on swash distribution are minimal. This is consistent with our findings from the two beach surveys conducted, where the slope measured

in June was similar to that measured in November (Figure 9).

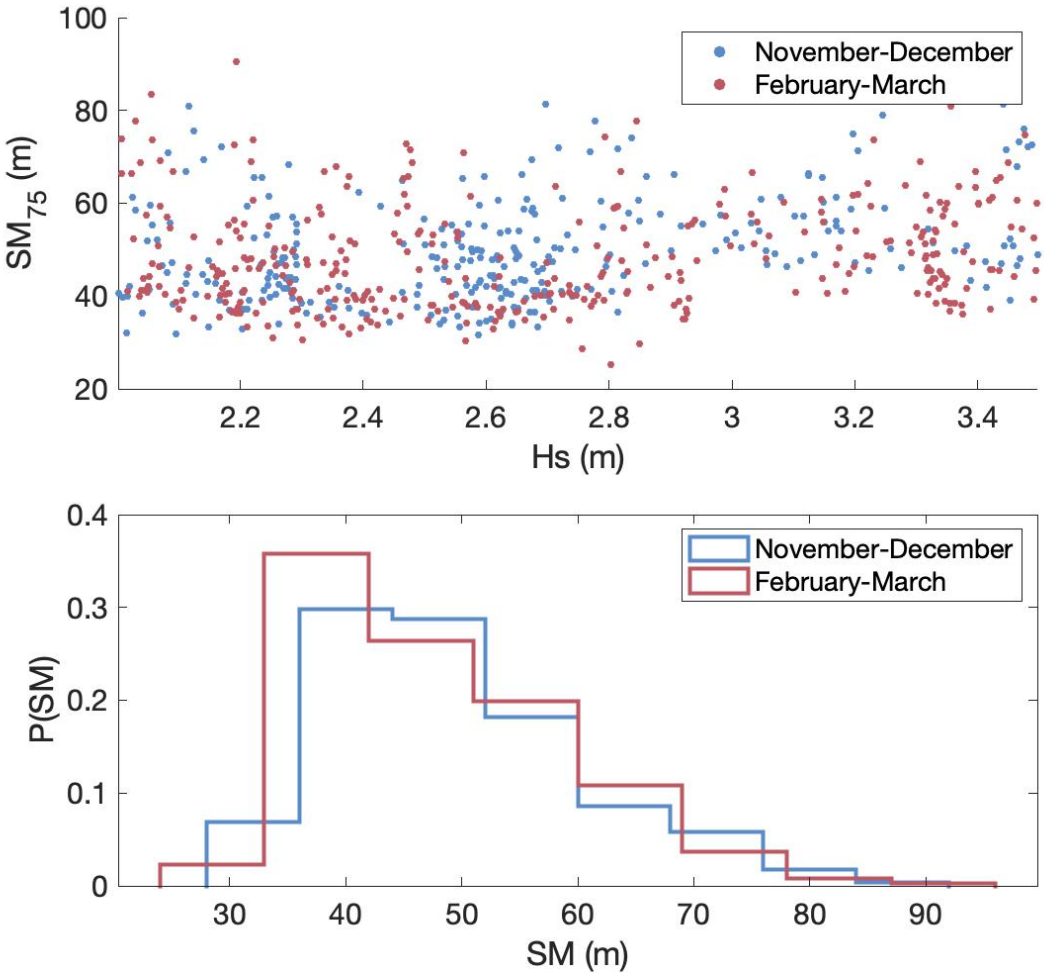

Figure 24: Top plot shows the binned SM_{75} for the start (Nov.-Dec.) versus the end (Feb.-Mar.) of the storm season as a scatter plot against Hs between 2.1m and 3.5m from La Perouse Bank wave buoy. Lower plot shows the distribution of SM_{75} for these two time periods.

Discussion

Case Study (October 2021)

In October 2021 we deployed a Spotter wave buoy in approximately 8 meter water depth along with an RBR pressure sensor. For approximately three weeks we have data from the MSC offshore wave buoy (LaPerouse Bank, C46204), our buoy and pressure sensor just outside the surfzone, and the onshore run-up timeseries from our camera. Using the additional measurements taken during this period, we will investigate further which sea-state variables determine wave run-up extent, and discuss the wave dynamics behind any observed relationships. Direct measurements of infragravity energy by the RBR pressure sensor allow us to show the role of these low frequency waves in determining run-up behaviour. Spectra from all data sources utilized in this case study are shown in Figure 25, and we see the RBR pressure sensor clearly resolving the infragravity signal that the wave buoys are unable to capture. Using these shallow water measurements collected over a few weeks, the most useful predictors for run-up are identified. These results are then used to propose practical ways to predict relative run-up strength using widely available offshore buoy data.

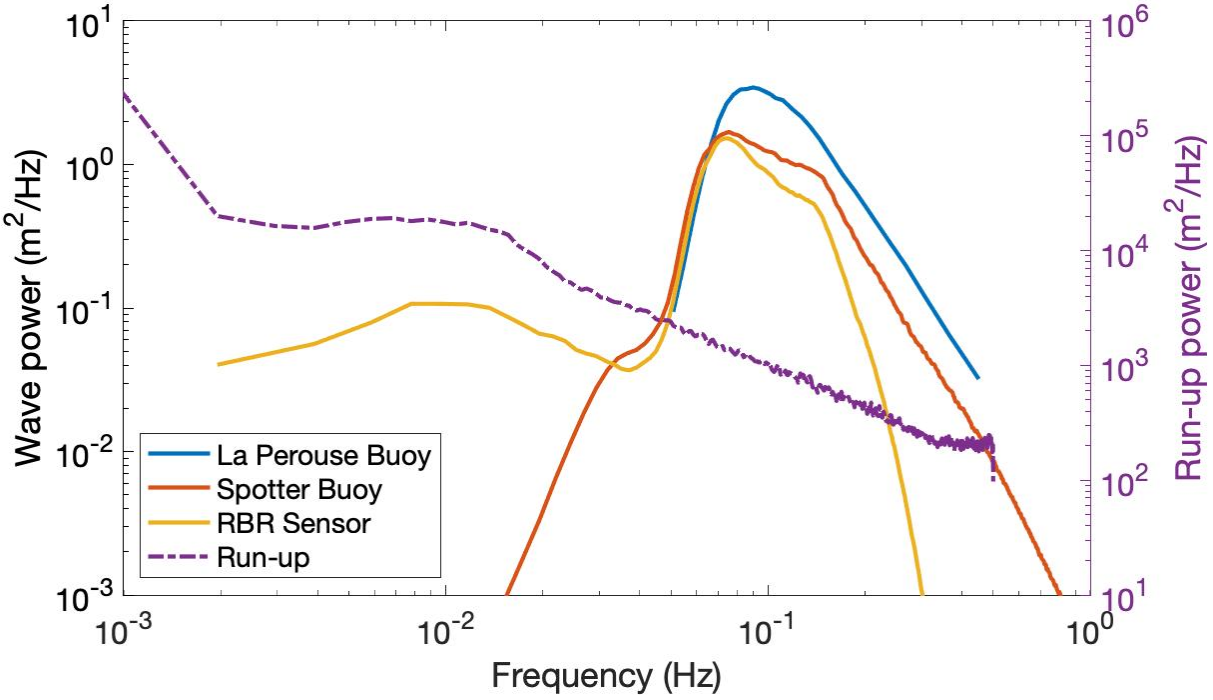

Figure 25: Spectra averaged over three week period that all instruments were simultaneously recording data. Left axis shows wave power for both wave buoys and the RBR pressure sensor. Run-up power (dotted purple line) is plotted against the right axis.

Figure 26 shows the correlation between the Hs and T0 data from the pressure sensor versus the Spotter wave buoy on the surface. Hs from the two sensors is shown to be precise, with an expected magnitude difference due to the inherent low-pass filtering associated with pressure data. The Spotter buoy on the surface consistently reads a higher wave height than the pressure sensor anchored on the bottom. Wave energy in a water column is a function of depth, and therefore the pressure sensor registers a lower wave height than a surface buoy. Wave periods between the two instruments are more accurate to each other than wave height, but there is a weaker correlation resulting from more outliers. Low frequency dominant periods recorded by the pressure sensor sometimes correspond with much shorter periods being calculated by the Spotter buoy. This likely occurs in sea states with multiple swells, the pressure sensor is more sensitive to long period swell whereas the Spotter buoy is picking up higher frequency motions as well.

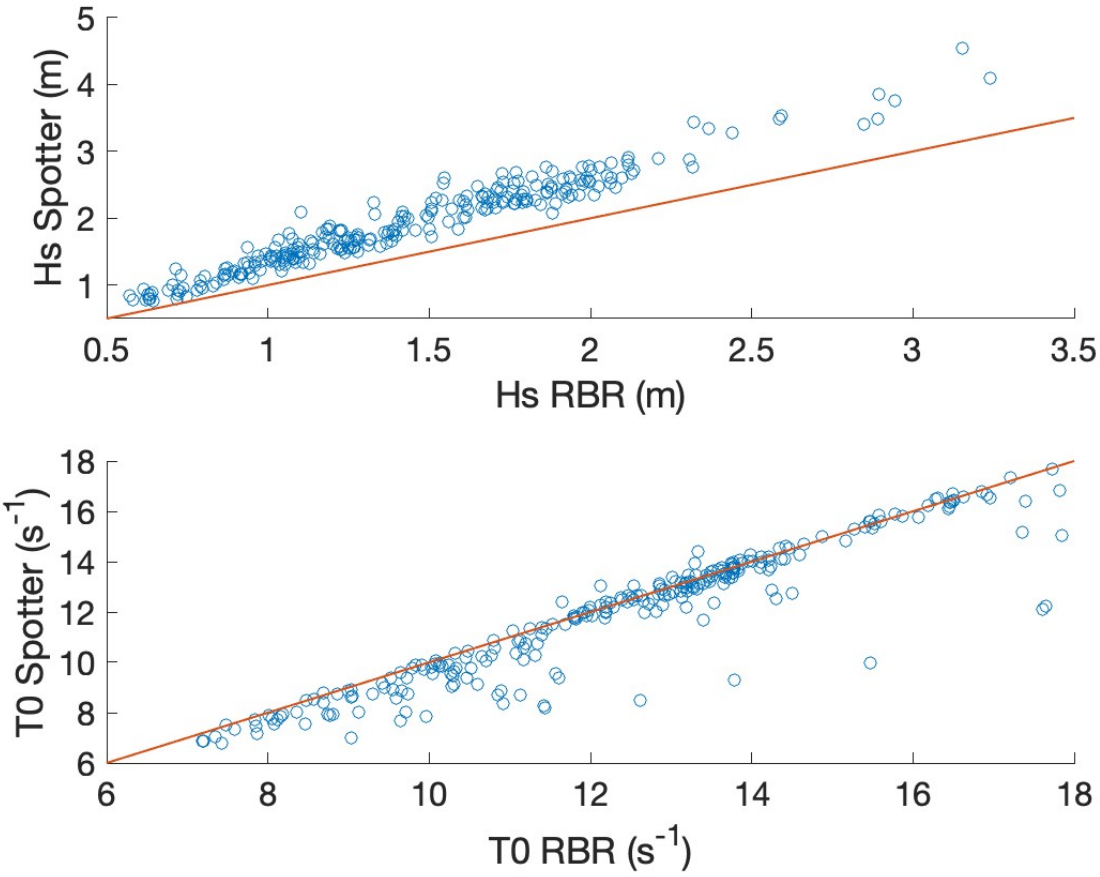

Figure 26: Comparison of the observations from the Spotter buoy (y-axis) and RBR pressure sensor (x-axis). Hs from the two sensors is scattered in the top plot, and T0 in the lower plot.

In Figure 27 below, SM_{75} is plotted against measurements from an RBR pressure sensor and Spotter wave buoy. Beach run-up is positively correlated to the significant wave height measured by both the RBR pressure sensor (Figure 27A) and the Spotter wave buoy (Figure 27B), with R values of 0.769 and 0.749, respectively.

Plots C and D in Figure 27 show SM_{75} plotted against $\sqrt{HL}$ calculated from the pressure sensor and wave buoy. While there is a correlation observed (R = 0.63 at RBR pressure sensor and R = 0.69 at wave buoy), it is weaker than the correlation with significant wave height alone. This is due to period being measured in water depths where many of waves measured are already undergoing breaking, rather than being measured in deep water.

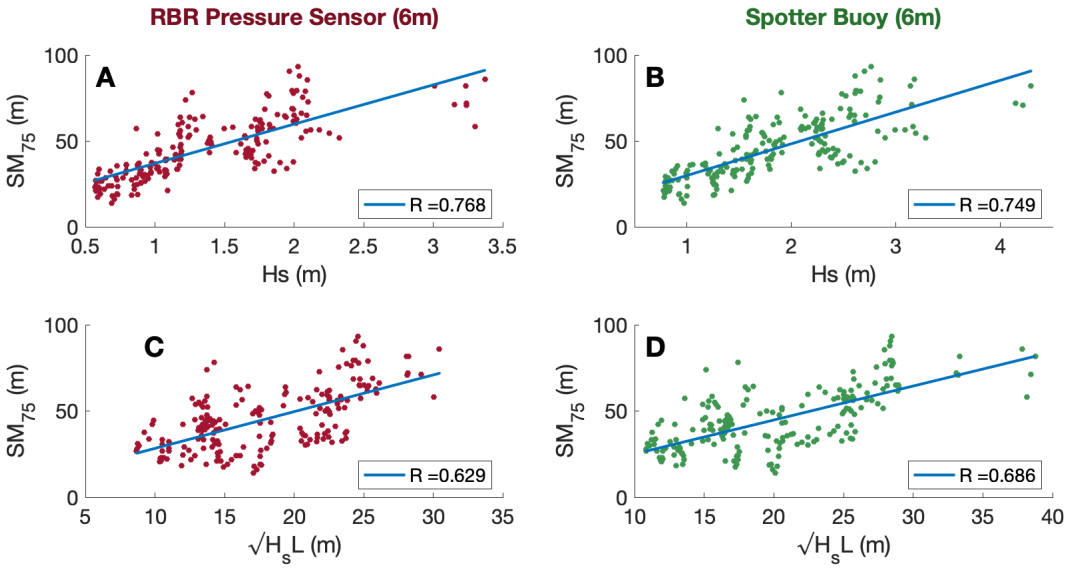

Figure 27: Correlations between SM_{75} and measurements from the RBR pressure sensor (left column) and Spotter wave buoy (right column) are shown. The top row plots swash maxima against Hs, and the bottom row $\sqrt{HL}$.

Unlike surface buoys, which filter out lower frequencies, pressure sensors are able to accurately capture the infragravity portion of wave spectra. Figure 28 shows the ratio between IG and SW energy in the spectrum versus wave run-up (SM_{75}). A correlation (R = 0.67) is observed, with higher relative IG energy in the spectrum leading to stronger run-up. Significant wave height is also plotted in Figure 28 using colour; visual observation of this plot shows a trend of low Hs points falling below the line of best fit and higher Hs points lying above.

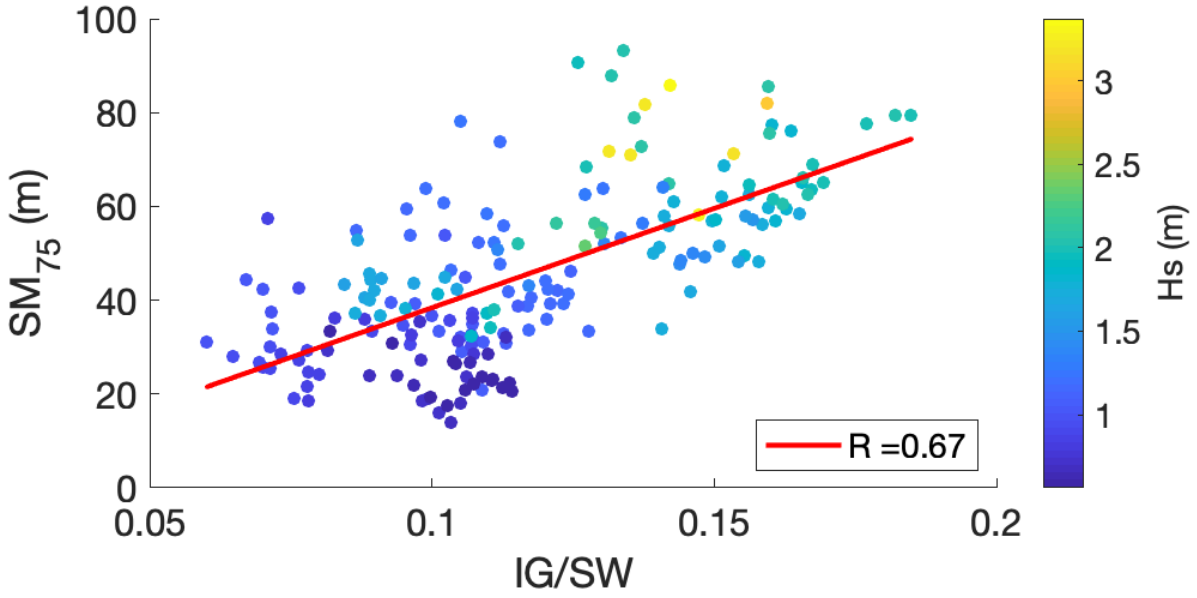

Figure 28: SM_{75} is plotted against the IG:SW ratio measured from the RBR pressure sensor deployed in approximately 6m water depth. The line of best fit is shown in red, with R = 0.67. The colour bar shows the significant wave height of each data.

By assuming that run-up is a function of both Hs and relative IG energy, and therefore multiplying these two variables together (see Figure 29), a stronger correlation between SM_{75} and sea-state variables is achieved (R = 0.803). This result shows that the strongest run-up will occur when periods of large Hs coincide with high relative IG energy in the wave spectrum.

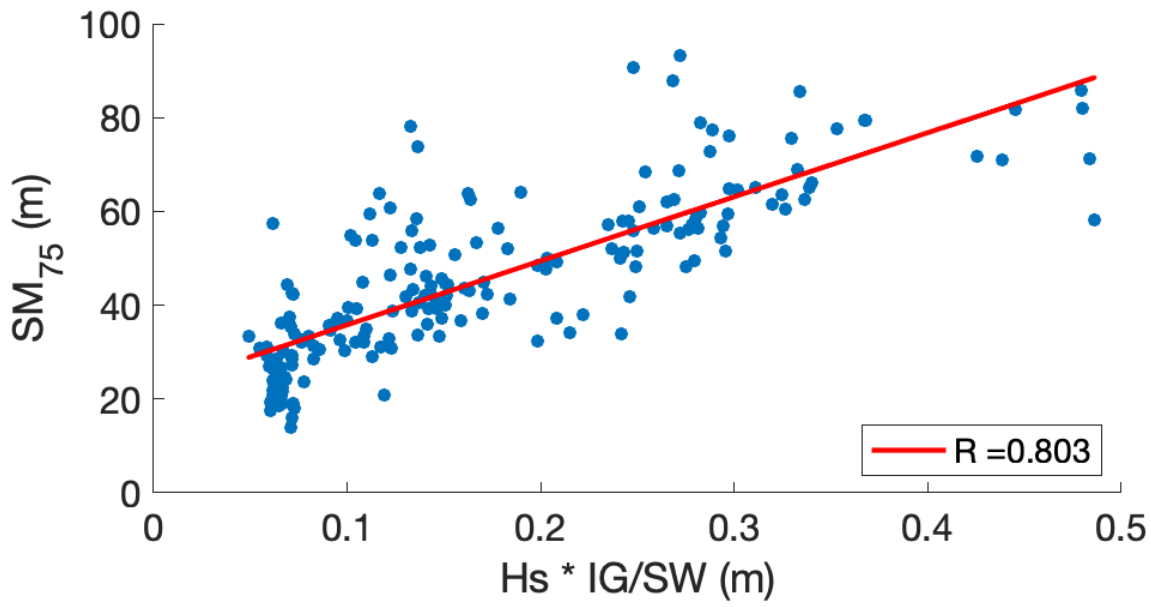

Figure 29: SM_{75} is plotted against the IG:SW ratio from the RBR pressure sensor multiplied by Hs.

Through measuring the wave field just outside the surf zone using a pressure sensor, we were able to show that run-up is dependant on the amount of IG energy in the spectrum. As wave buoys are unable to resolve IG frequencies, for this result to be useful in application it is necessary to find a suitable proxy or estimate of IG energy in the incoming wave field. It is assumed that the dominant source of these observed IG waves at 6m water depth is the bound wave generation mechanism. The varying breakpoint mechanism is unlikely to be significant on such a dissipative beach, and the pressure sensor was likely too deep to be measuring edge waves (which are trapped near the beach). This does not exclude bore-bore capture as a factor in wave run-up, but as the sensor was located outside of the typical surf zone, the IG motions observed would not have been driven by capture events. In assuming that bound IG waves associated with wave groups generate the observed IG signal, we look for measures of 'groupiness' to improve our estimates of SM_{75}.

The parameter 'r' is a measure of the crest-trough correlation of a wave field, and is correlated to groupiness (Häfner et al., 2021). The crest-trough correlation r can be calculated from the 1-D wave spectrum using equation 7.

$$r = \frac{1}{m_0}\sqrt{\rho^2 + \lambda^2} \tag{7}$$

Where,

$$\rho = \int_0^\infty S(f)cos(2\pi f\tau)df, \qquad \lambda = \int_0^\infty S(f)sin(2\pi f\tau)df$$

Figure 30 looks at the relation between this crest-trough correlation parameter and the IG:SW energy ratio from the RBR pressure sensor. The line of best fit is calculated from $r > 0.5$ and shows that crest-trough correlation is positively correlated to the IG:SW energy ratio and therefore may be a useful proxy for the infragravity wave magnitude in the absence of direct measurements from a pressure sensor.

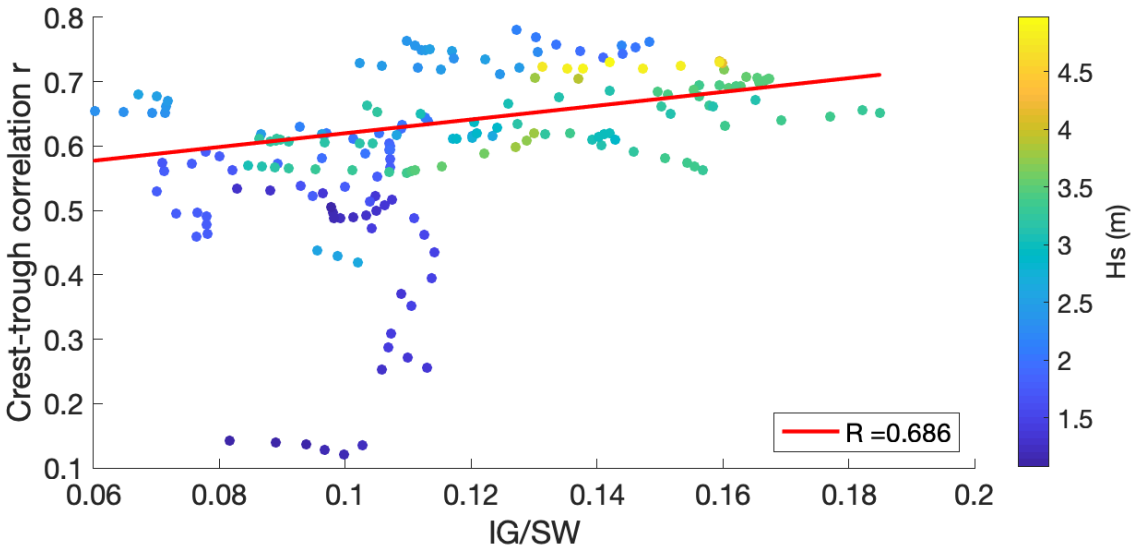

Figure 30: The crest-trough correlation parameter r is calculated from La Perouse Bank wave buoy and plotted against the IG:SW ratio measured by the RBR pressure sensor. The colour bar shows the corresponding Hs (from La Perouse Bank) for each data. A line of best fit (in red) is calculated for $r > 0.5$.

Figure 31 shows SM_{75} plotted against r calculated from the Spotter buoy spectra (top) and the La Perouse Bank buoy spectra (bottom). The value for r calculated from the Spotter buoy is poorly correlated to run-up, with lower crest-trough correlation values for large Hs compared to the offshore buoy. This is because large waves have already begun shoaling by the time they reach the Spotter buoy, leading to a loss of the group wave structure and decreased crest-trough correlation. The crest-trough correlation is used as a proxy for the infragravity motion resulting from the wave group, when the group structure is lost through wave breaking the previously bound infragravity wave is released and continues

to propagate towards the shore. For this reason, crest-trough correlation becomes a poor approximation for infragravity energy in shallow water. There is a good correlation (R = 0.54) when calculating r from the offshore wave buoy, demonstrating that this would be a useful parameter to be incorporated into run-up estimates alongside Hs.

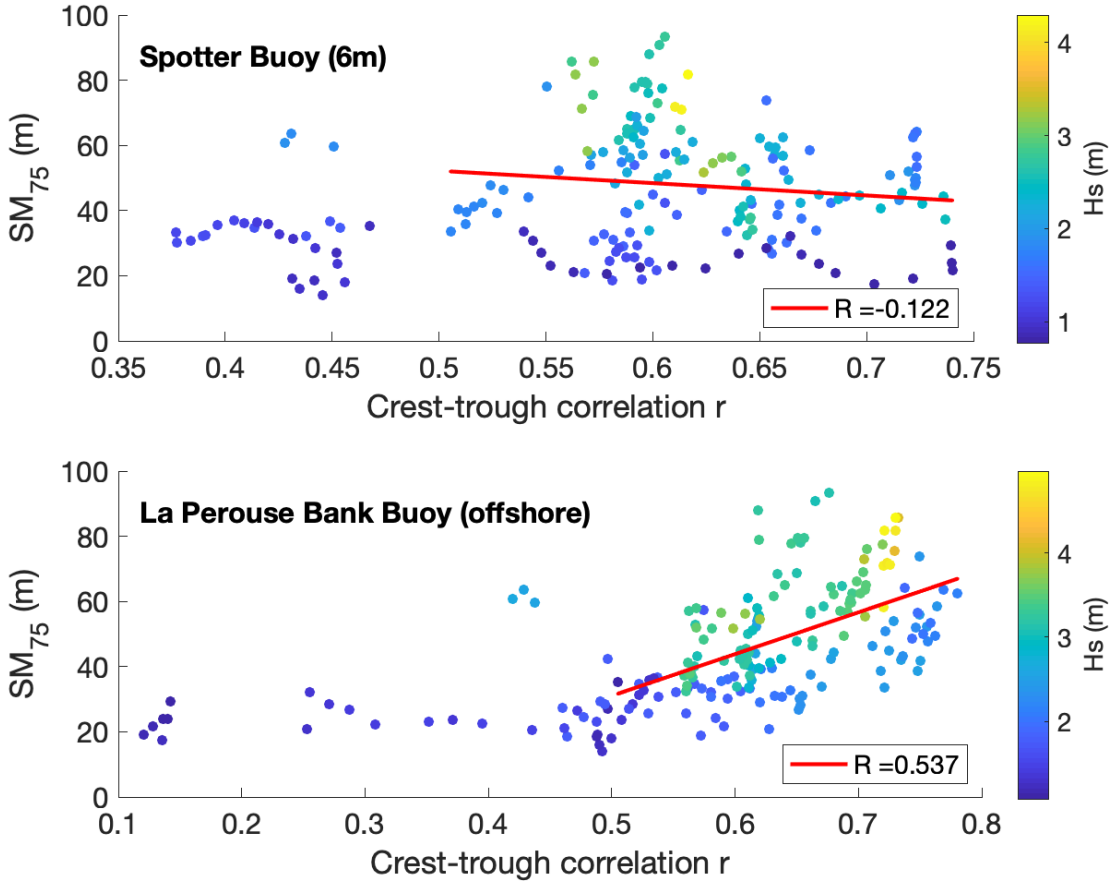

Figure 31: SM_{75} is plotted against crest-trough correlation parameter r, with the colour bar showing the corresponding Hs for each data. Top plot uses observations from the Spotter wave buoy, and lower plot uses observations from the offshore La Perouse Bank wave buoy. A line of best fit (in red) is calculated for $r > 0.5$.

The correlation between SM_{75} and Hs observed at La Perouse Bank (Figure 32, upper panel) has an R-value of 0.75, which is similar to the correlations for Hs calculated from the pressure sensor (R = 0.768) and Spotter buoy (R = 0.749). This finding is interesting as it suggests that there is little benefit to using shallow-water sensors when estimating SM_{75} from Hs alone. It is however possible that this is due to the limited duration of the case

study, and local sensors may prove to be more useful when tested over a longer period and under a variety of sea conditions.

The bottom panel of Figure 32 shows an improvement in run-up estimations when Hs is multiplied by r with a resulting R of 0.788. This finding indicates that in the absence of more direct measurements of IG energy, the crest-trough correlation can be utilized as an indirect measurement of the IG signal via wave groupiness.

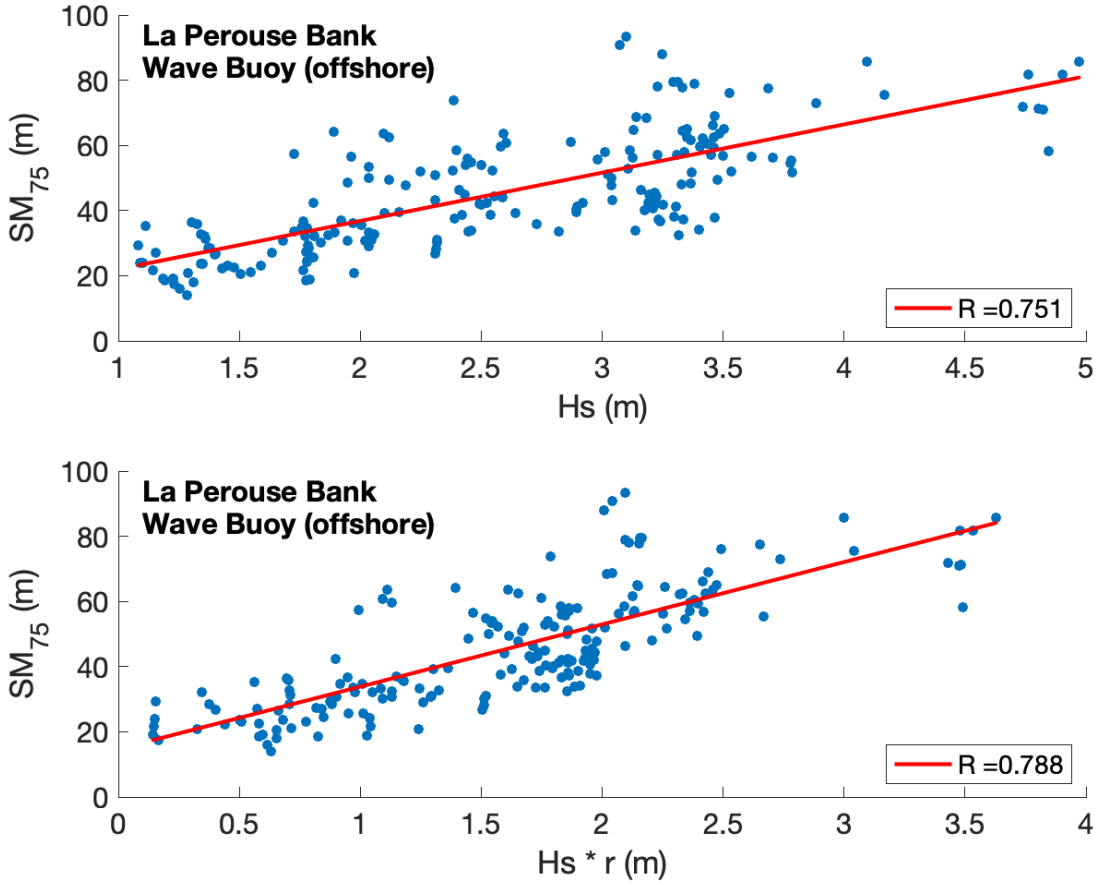

Figure 32: Using measurements from the La Perouse Bank wave buoy, SM_{75} is plotted against Hs (top plot) and Hs * r (lower plot).

In Figure 27, $\sqrt{HL}$ performed poorly compared to Hs in predicting SM_{75} as a result of the wave period being measured in shallow water. When calculating L from offshore wave field measurements as intended, $\sqrt{HL}$ performs better than Hs (Figure 33). There is also a notable improvement in correlation to SM_{75} when $\sqrt{HL}$ is multiplied by r, R = 0.778 to R

= 0.835.

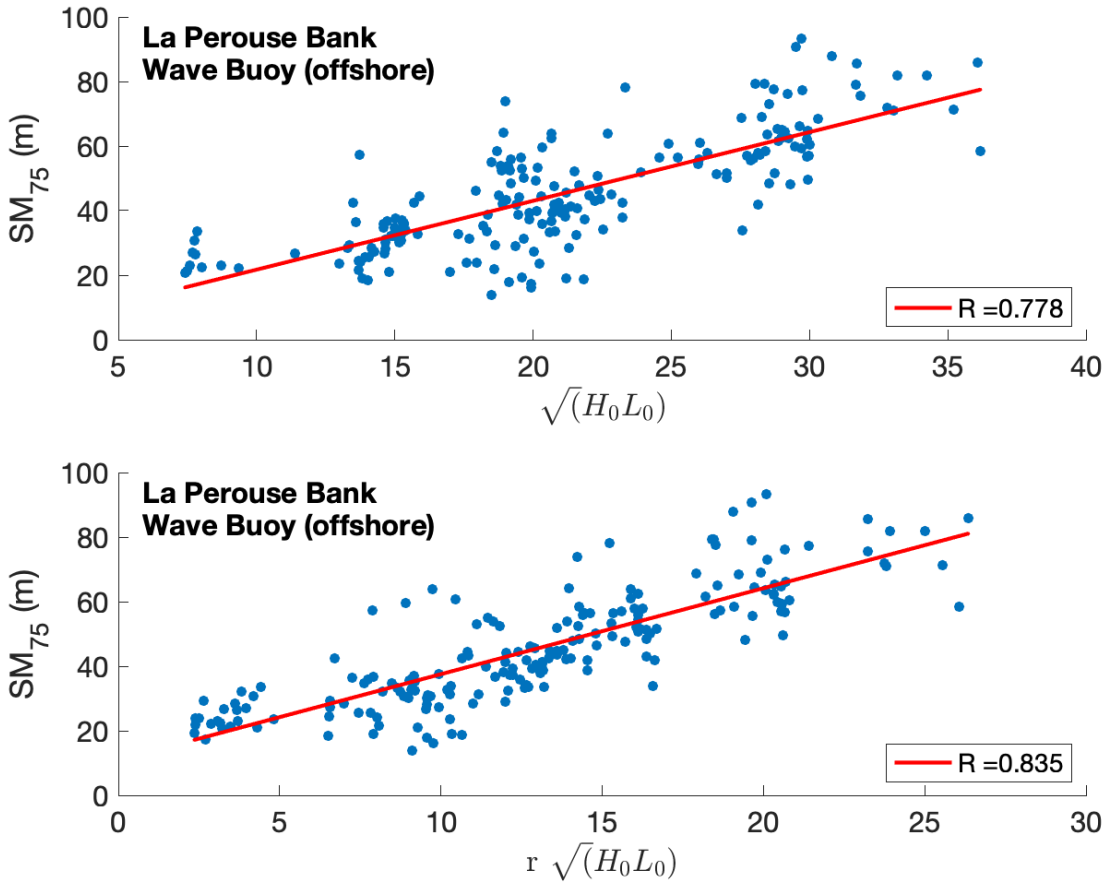

Figure 33: Using measurements from the La Perouse Bank wave buoy, SM_{75} is plotted against Hs (top plot) and Hs * r (lower plot).

Similar results are found when using data beyond the three week case-study period (Figure 33). The parameter $\sqrt{HL}$ is a stronger predictor of run-up (R = 0.635) than Hs (R = 0.52). Correlation is improved when multiplied by r for both $\sqrt{HL}$ and Hs, R = 0.629 and R = 0.524 respectively, although these improvements in predicting power are less significant than seen in the case study.

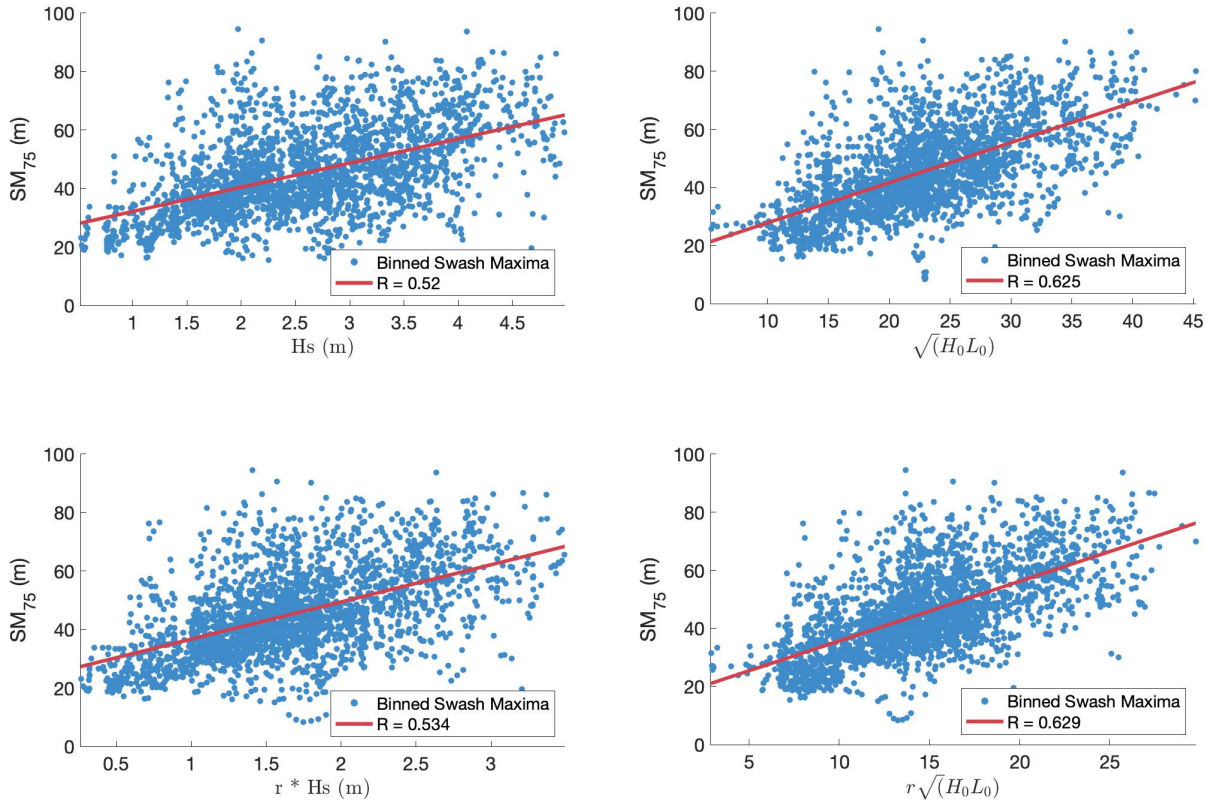

Figure 34: SM_{75} is plotted against the Hs (top left), r * Hs (bottom left), $\sqrt{HL}$ (top right), and $r\sqrt{HL}$ (bottom right). Red line is linear best fit.

Other potential proxies of infragravity energy were explored in addition to crest-trough correlation r. The Smoothed Instantaneous Wave Energy History (SIWEH) based groupiness factor (Mansard and Funke, 1980) also approximates the bound infragravity wave in a wave group, but is calculated from sea-surface elevation and is therefore not practical for buoy observations that only record and transmit wave spectra. Spectral bandwidth was also tested and found to be a weaker predictor of wave run-up than r.

Using the infragravity data collected during the three week period of RBR pressure sensor deployment, we see that infragravity energy is a strong predictor of run-up behaviour. In the absence of direct measurements of infragravity energy, proxies for these low frequency motions can be utilized to account for this mechanism. Crest-trough correlation (r) is shown to be a useful proxy, as it is calculated from the 1-D wave spectrum and improves run-up estimates when included in a function with $\sqrt{HL}$. There is a smaller improvement in correlation from $\sqrt{HL}$ to $r\sqrt{HL}$ when using the bulk data versus the limited case-study data, suggest-

ing that the usefulness of r may differ across wave environments. Having demonstrated the potential for r in improving run-up predictions, future work should explore better ways to include r in wave run-up parametrizations to optimize its utility.

Investigating Bore-Bore Capture as a Driving Mechanism of Extreme Run-up

The previous section showed the correlation between run-up magnitude and the amount of IG energy in the incoming wave field, and discussed practical ways to incorporate this variable into run-up predictions. The process of bore-bore capture has been shown to drive extreme run-up events on dissipative beaches (Tissier et al., 2015; García-Medina et al., 2017; Stringari and Power, 2020). Bore-bore capture requires that bores are propagating across the surf-zone close enough together to be able to interact and merge. This means that during lower energy sea-states, where waves are breaking closer to the beach and resulting bores are small and dissipate quickly, extreme run-up events are small and infrequent. Higher energy sea-states being more favourable to bore-bore captures is a likely factor in why large run-up is observed during energetic wave conditions. Bore-bore capture also requires irregularity in bore size, and therefore propagation speed, of bores in the surf-zone. Infra-gravity waves introduce variability in water depth, and therefore bore propagation speed, and facilitate more capture events than would otherwise occur.

While some bores will dissipate across the surf zone, it is important to note that the IG signal in the run-up spectrum is not solely due to a net loss of waves. Figure 35 shows the averaged spectra for run-up during high (Hs $>$ 3m) and low (Hs $<$ 3m) sea states.

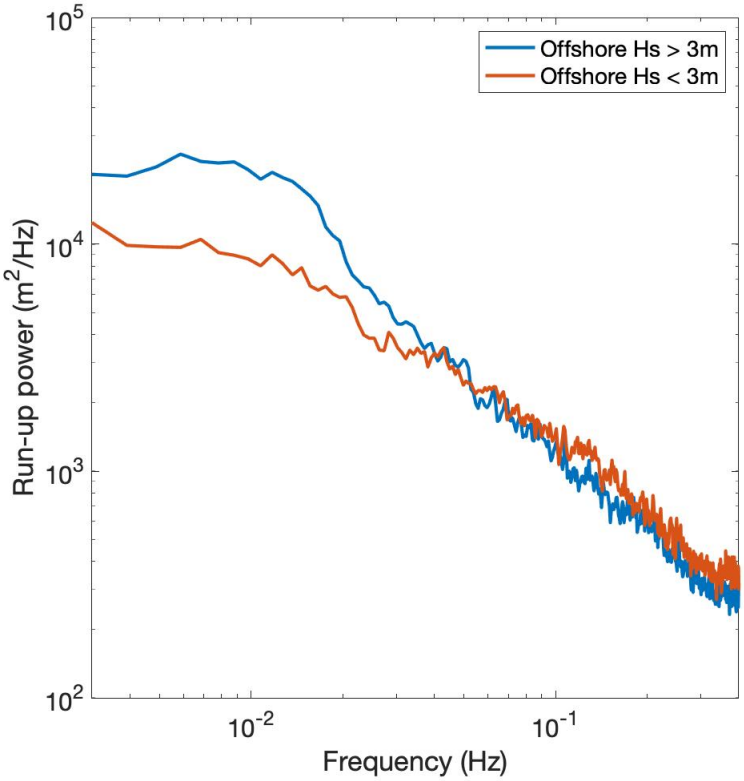

Figure 35: Averaged run-up spectrum from sea-states where Hs is over 3m (blue line) and under 3m (red line).

If dissipation alone was driving down the peak period of run-up to lower frequencies, then we would expect to see peak periods more similar to wind-wave frequencies when the incoming wave field was energetic. This is because as wind-waves break and dissipate across the surf-zone, the loss of the signal at wind-wave frequencies in the resulting run-up spectrum and apparent peak frequency in the IG range could be solely due to differential dissipation of wavelengths. The IG peak frequency in the run-up spectra occurring at both low and high energy sea-states suggests that there is a mechanism shifting wind-wave energy into lower frequencies and that the observed spectral shift cannot be only driven by dissipation.

Without direct measurements of IG energy across the surf zone, it is difficult to conclusively determine the cause of the IG signal present in the run-up spectrum. While bore-bore capture can occur in the absence of other IG waves and lead to a spectral shift to lower frequencies, capture events can also be facilitated by the presence of IG wave motions in shallow water. If a wave or bore occurs on the crest of an IG wave, it will gain momentum

and travel towards the beach with more energy. Through this same mechanism of differentially increasing the propagation speed of waves/bores in the surf zone, IG motions facilitate capture events where the energy of two bores is combined. When the resulting bore from the capture runs up the beach, it can cause a higher than average shoreline maxima. For this reason, the IG signal measured immediately outside of the surf zone, where capture events are not yet occurring, does not rule out the potential contribution of bore-bore capture to the IG signal observed in the run-up spectrum.

Using the video footage of run-up at high-tide we can measure how the dominant periods shift in the swash zone. Rather than tracing the interface between water and sand, the timestack is binarized and the spectra are calculated from the resulting timeseries at four locations along the transect (Figure 36).

The corresponding observed wave spectra are also plotted, and show that the incoming wave field has a peak period of 10 seconds. The timestack spectrum from the first location (30) has dominant periods between 10 and 20 seconds, but the dominant period shifts to lower frequencies with each subsequent position moving up the beach. This shows that the spectral transformation of the wave field is not uniform across the course of the surf zone, but rather the changes observed happen quite rapidly in the extremely shallow and onshore regions of the transect.

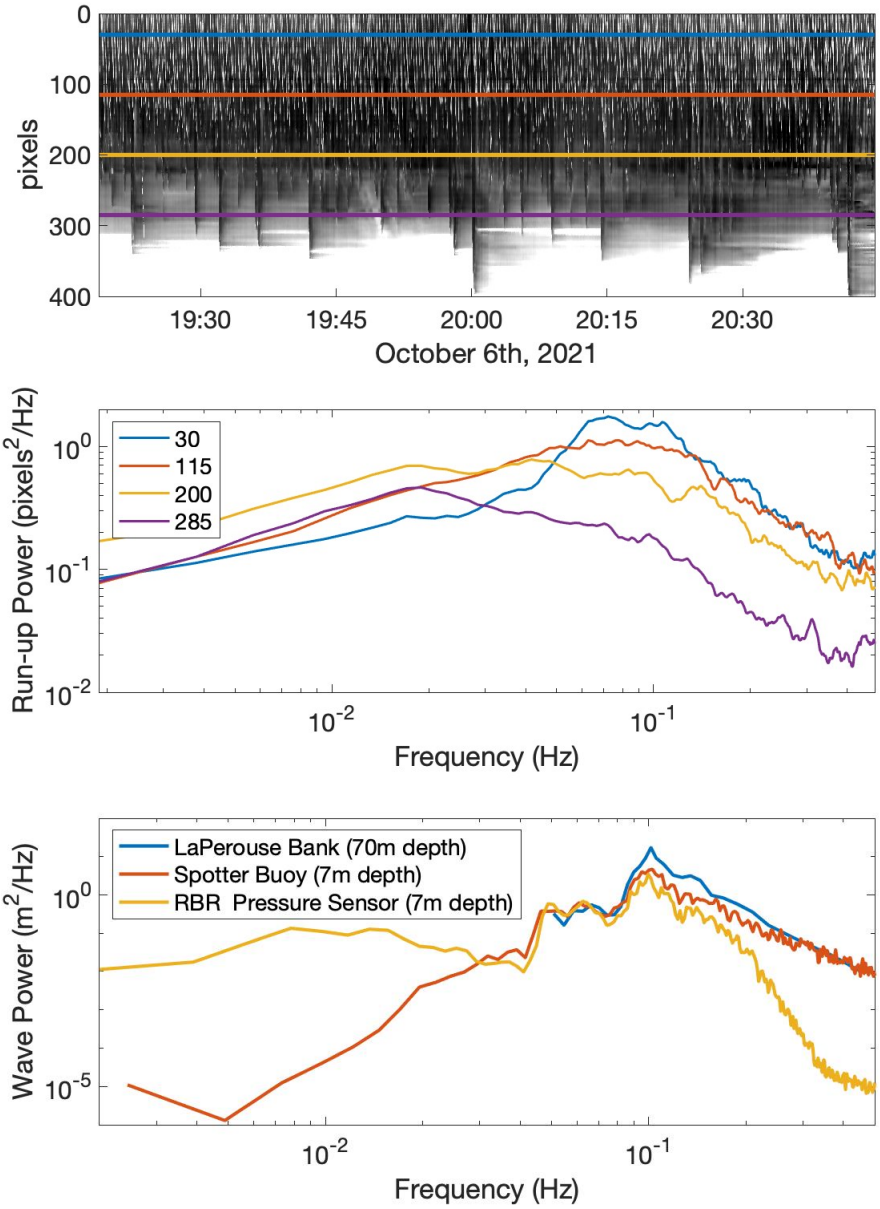

Figure 36: Wave spectra calculated from five different points of the incoming run-up (top figure). Data were binarized for each "slice" and the spectrum was calculated from the resulting timeseries (middle figure). Bottom figure shows wave spectra observed over the same time period.

If bore-bore capture is a significant contributor to the IG signal observed in the run-up spectrum, then we would expect rapid spectral transformation in the swash zone as seen in Figure 36. Since capture events are driven by differing propagation speeds between two

bores, more captures will occur as the individual bore height becomes increasingly important relative to the total water depth. This is consistent with what we see in the data and a likely explanation for the spectral shifts observed in Figure 36.

Simple BBC Model

Bore-bore capture occurs when a bore (broken wave) catches up with the bore in front of it, and is the direct result of varying propagation speeds from bores with different heights. The result of this bore-bore capture is a merging of the two bores and their respective heights being combined; this single bore then continues its propagation towards the beach. This phenomena provides a mechanism for the shape of the spectra seen at the beach: bores combine together to effectively increase the average period of the "wave" field and shift energy into lower frequencies. The following section employs a conceptual simulation of bore-bore capture to study how this process impacts run-up on the beach under varying sea-states.

BBC Model Methods

A simple numerical model propagates waves and bores towards the beach, the workflow can be seen in the diagram 38. Positive sea surface heights are input at a location away from the shore (900 meters out) and then the model moves the wave/bore forward in space and time towards the beach.

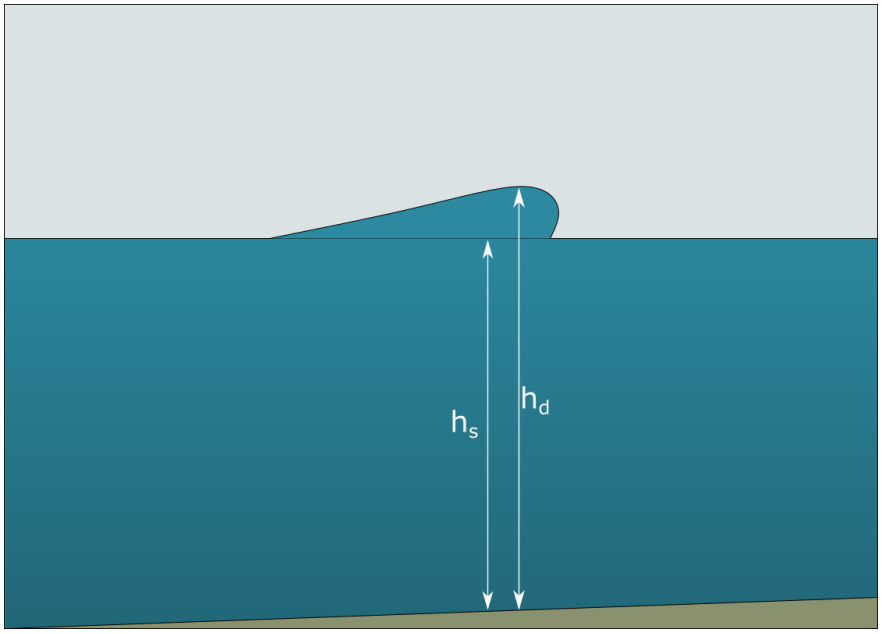

Figure 37: Bore heights: h_s is the undisturbed local sea level, h_d is equal to h_s plus the additional sea surface elevation from the disturbance (amplitude, in the case of a wave).

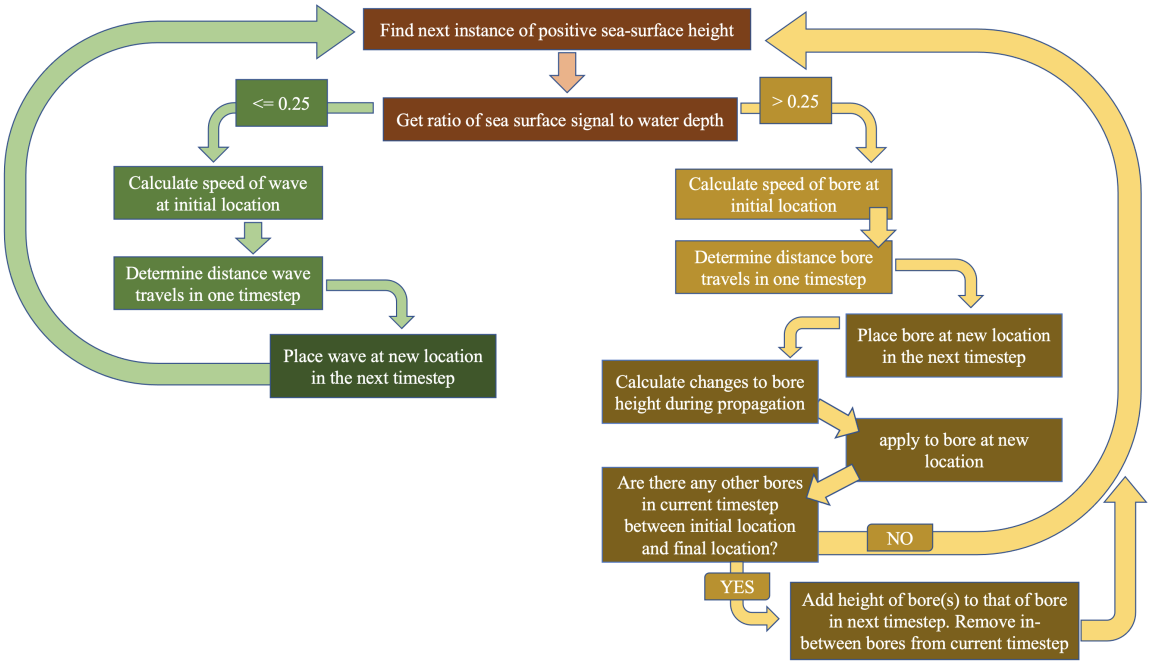

Figure 38: Work flow for model.

Waves do not lose any height as they approach the shore, and are able to pass through

each other. Their speed is determined by the equation for shallow water waves:

$$c_{wave} = \sqrt{g(h_s)} \tag{8}$$

Where h_s is the average water depth and g is the acceleration due to gravity. Wave breaking occurs according to the ratio between h_s and h_d (see Figure. 37), once a wave becomes too high relative to the depth it is treated as a bore. If a signal is flagged as a bore during any point during its propagation it can not revert back to a wave, even if its height is reduced enough to satisfy the wave ratio. Bores propagate at a different speed and lose energy due to friction. The equation for bore velocity, c_{bore}, is given by Freeman and Lemehaute (1964) (equation 9). Bores also combine together when they coincide, which represents the bore-bore capture we are trying to simulate.

$$c_{bore} = \sqrt{\frac{g}{2}(h_s + h_d)\frac{h_d}{h_s}} \tag{9}$$

After the bore is moved forward a new speed is calculated according to equation 10:

$$c_{bore2} = c_{bore1} - a\Delta t \tag{10}$$

where $a = g\mu\frac{h_d}{h_s}$ represents the dissipation that occurs to a bore. Bore dissipation is dependent on both water depth and bottom roughness, which is included in this model as a tunable parameter μ. Equation 9 can then be rearranged to solve for a new total depth (h_{d2}) using c_{bore2} and h_{s2}. The height of the bore at the new location becomes $h_{d2} - h_{s2}$.

Testing model with single waves

Figure. 39 shows high and low resolution model outputs for different wave heights and friction coefficients (μ). The average bore height at the beach is consistently higher for low spatial/temporal resolution model runs than compared to high resolution runs. The differences between high and low resolution runs are also positively correlated to input wave height and negatively correlated to μ. Using a low dissipation parameter results in large bore heights at the beach which are primarily dependent on the input Hs, and a large (40 cm) difference between high and low resolution model runs. Setting μ to 0.005 takes a lot of the energy out of the waves as they propagate towards beach. The result is low bore heights onshore with small differences in bore heights between different Hs inputs. An aspect of the model where problems could arise is the propagation in very shallow water. The bore height

decreases quickly near the beach, and the final bore height output is very sensitive to each time-step. For this reason, the finer resolution is preferred as it minimizes this source of error and better allows us to capture a realistic bore height at the beach. While the low resolution runs can reasonably model the wave/bore over the entire course of its propagation, Figure 39 shows how the low resolution model is too coarse to capture the rapid dissipation of bores as they move into shallow water.

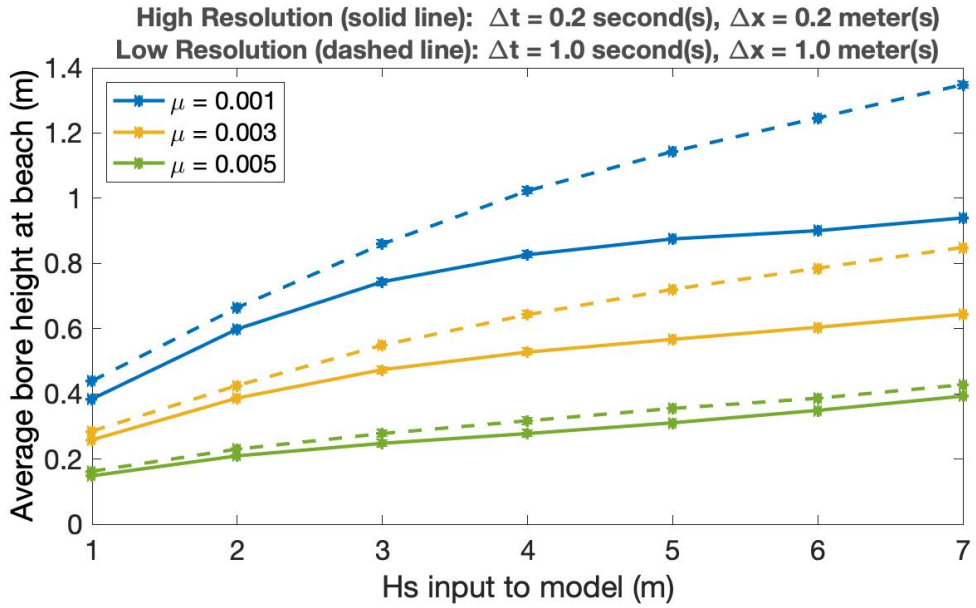

Figure 39: Initial and final heights of waves for high resolution model run (solid line) and low resolution model (dashed line).

The momentum of waves as they move into shallow water can result in the wave height actually increasing, particularly when energy loss due to dissipation is low. This behaviour is consistent from a physics point of view, but waves/bores increasing drastically (by a couple meters) is unlikely. A friction coefficient ($\mu = 0.003$) was chosen for the rest of the model runs input with "real" data; this selected value prevents significant wave growth while not being so high as to reduce all wave heights to 0 by the time they reach the beach (figure. 40).

Model Results and Discussion

Synthetic wave fields are generated from JONSWAP spectra with various significant wave heights. Figure 41 shows the model output with input of waves calculated from these synthetic surface elevation timeseries. The inset bar plot shows the total number of waves

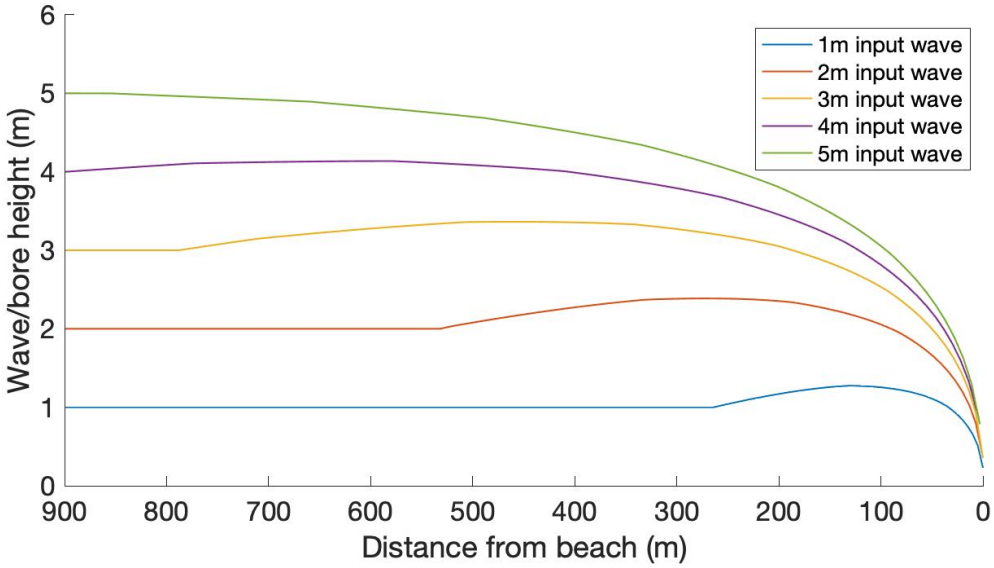

Figure 40: Wave/bore height evolution during propagation into shallow water for model input wave heights 1 to 5 meters.

input versus the total excursions at the beach, with the yellow portion being the number of bore-bore captures. Here we see that the number of bore captures increases relative to both the number of waves input and output with increasing significant wave height. We also see that the majority of the waves reaching the beach under energetic sea-states have captured another bore at some point during its propagation across the surf zone. While this plot shows BBC instances as a proportion of number of waves output, total BBC could actually exceed waves output if two bores merged and then dissipated before reaching the beach.

The lower plot in Figure 42 illustrates the transect that the model waves propagate across and corresponding water depths. The upper panel shows the cumulative sum of bore captures over the transect for the three different Hs scenarios. Here we see that the total number of bore-bore captures increases with Hs, and that these captures begin occurring earlier (in deeper water) than when Hs in lower. This is because captures only begin occurring when the wave height to water depth ratio is high enough to undergo 'breaking'. During 1.5m Hs sea-states, waves do not break until around 6m water depth, and then the cumulative sum of captures increases steadily until the beach. When sea-states are large (Hs = 5m) bore captures begin occurring in 10m water depth and steadily increase until approximately 7m water depth, at which point the number of captures begins to plateau. This indicates a saturation in BBC events, with a cascade of captures occurring initially until the bores

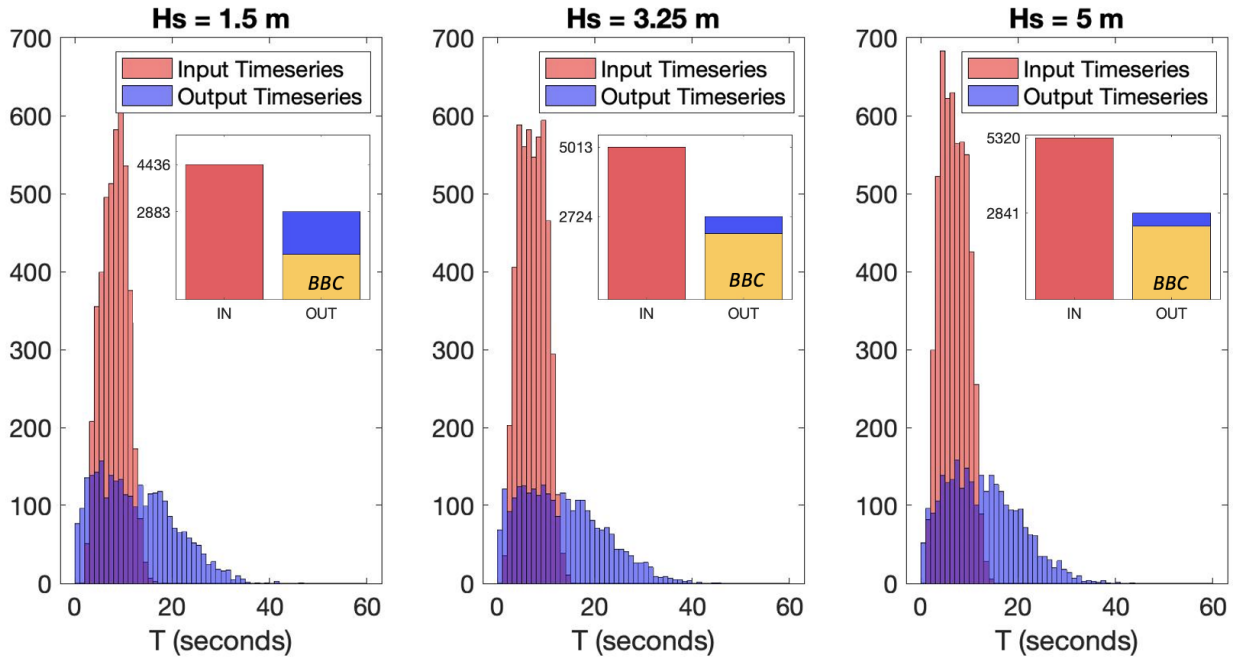

Figure 41: Distributions of input wave heights and the corresponding output bore heights. Model runs with significant wave heights of 1.5m, 3.25m, and 5m are shown, as well as the number of bore captures that occurred over the course of propagation.

become too spread out for more merging to occur. In shallow water depths (<2m), the rate of captures increases again as the bore's height relative to total water depth becomes significant enough to lead to more variance and drive additional captures.

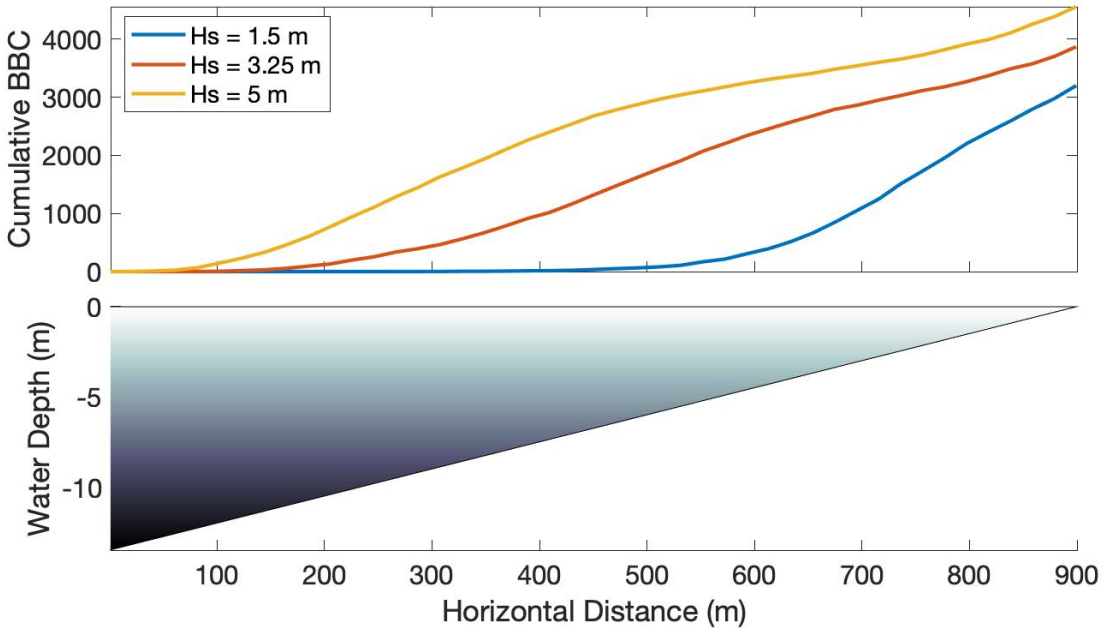

Figure 42: Top panel shows the cumulative number of captures in simulations runs with three different significant wave heights. Bottom panel shows the beach slope used in the simulation.

This simulation demonstrates how bore-bore capture alone could play a significant role in altering the wave field within the surf zone across a variety of sea-states. We also see how the merging of bores can drive extreme events, particularly when occurring in the most landward extent of the transect. Infragravity waves are not included in this simulation, but would be expected to increase the rate of captures by adding variability to bore heights across the surf-zone. These results are consistent with the shift from wind-wave to lower peak periods in our run-up observations.

Conclusion

Run-up spectra and statistics collected using video footage have been presented as well as wave field measurements taken in both shallow and deep water. The run-up spectra consistently have a peak period in the infragravity range and a spectral roll off around $f^{-1.5}$, which differs significantly from the typical wind-wave periods and frequency dependence of f^{-4} that is observed offshore. This spectral shape featuring a dominant infragravity signal was observed across all sea-state conditions. The transformation of the spectra occurs across the entire surf-zone, but most rapidly within the furthest landward extent of the surf-zone and swash-zone.

Run-up was found to be larger when there was a greater amount of infra-gravity energy relative to short-wave energy in the incoming wave field entering the surf-zone. Multiplying Hs by the IG:SW energy ratio improved the correlation to SM_{75} over using Hs alone (R=0.803 versus R=0.768). Considering how difficult direct measurements of IG energy are to obtain, parameters for wave groupiness were explored as indirect estimates of relative IG energy in the wave field. The crest-trough correlation parameter r, which is correlated to groupiness, was used as a proxy for IG energy in the wave field. Using wave buoy data from La Parouse Bank, it was shown that including r in a parametrization with $\sqrt{HL}$ improves the correlation to SM_{75}. This improvement was significant in the three week case study data (R=0.778 for $\sqrt{HL}$, R=0.835 for $r\sqrt{HL}$), but relatively minor when applied to the entire run-up data. This suggests that the predictive power of r varies across different wave conditions and that more calibration is required to improve utility.

Capture events could be visually identified in the video footage of our study area, and a simple simulation showed that BBC alone could drive extreme run-up events and a significant spectral shift towards lower frequencies. The presence of infragravity waves within the surf-zone facilitate increased BBC, supporting our finding that a higher ratio of IG to SW energy in the wave spectrum contributes to larger run-up instances on the beach.

Long-term in-situ observational studies have limitations in the ability to control or ac-

count for all variable factors in the environment. While some measurements of bathymetry and beach slope were taken and appeared reasonably consistent, it is possible that storms were driving changes in beach morphology on the timescale of days that may have shown up in the run-up data but were unable to be attributed to bathymetrical shifts due to the absence of data. Future studies should aim to control for this variable by choosing a site where beach morphology can be assumed constant, possibly a rockier beach, and justify this assumption by taking bathymetry measurements before and after a storm event to show that any changes in morphology are minor and can be ignored moving forward. Shifting beaches could also be accounted for by frequent bathymetry surveys throughout the duration of the study, particularly around storm events where the most drastic changes can be expected.

While it has been shown here that IG waves likely play a strong role in run-up behaviour based on measurements of IG energy at the edge of the surf-zone and the presence of an IG signal in the run-up data, it would have been beneficial to have more observations of IG energy. To characterize the evolution of IG waves in shallow water, future in-situ studies could deploy instruments across various depths in the surf-zone that measure IG wave magnitude, and ideally even direction. Future work in this field should include in-situ observations of run-up across a variety of beach environments to study spectral transformation and the role of BBC in the surf and swash zone.

Bibliography

Ardhuin, F. and Orfila, A. (2018). *Wind Waves*, pages 393–422. CreateSpace Independent Publishing Platform.

Battjes, J. (1974). Surf similarity. *Coastal Engineering Proceedings*, 1(14):26.

Battjes, J. A., Bakkenes, H. J., Janssen, T. T., and van Dongeren, A. R. (2004). Shoaling of subharmonic gravity waves. *Journal of Geophysical Research: Oceans*, 109(2):1–15.

Beaugrand, H. (2010). Beach-dune morphodynamics and climate variability impacts on wickaninnish beach, Pacific Rim National Park Reserve, British Columbia, Canada. Master's thesis, University of Victoria.

Bergsma, E. W., Blenkinsopp, C. E., Martins, K., Almar, R., and de Almeida, L. P. (2019). Bore collapse and wave run-up on a sandy beach. *Continental Shelf Research*, 174(August 2017):132–139.

De Bakker, A. T., Tissier, M. F., and Ruessink, B. G. (2016). Beach steepness effects on nonlinear infragravity-wave interactions: A numerical study. *Journal of Geophysical Research: Oceans*, 121(1):554–570.

Dodet, G., Melet, A., Ardhuin, F., Bertin, X., Idier, D., and Almar, R. (2019). The Contribution of Wind-Generated Waves to Coastal Sea-Level Changes. *Surveys in Geophysics*, 40(6):1563–1601.

Fiedler, J. W., Young, A. P., Ludka, B. C., O'reilly, W. C., Henderson, C., Merrifield, M. A., and Guza, ·. R. T. (2020). Predicting site-specific storm wave run-up. 104:493–517.

Freeman, J. C. and Lemehaute, B. (1964). Wave breakers on a beach and surges in a dry bed. *Journal of Hydraulic Engineering*, 90:187–216.

García-Medina, G., Özkan-Haller, H. T., Holman, R. A., and Ruggiero, P. (2017). Large runup controls on a gently sloping dissipative beach. *Journal of Geophysical Research: Oceans*, 122(7):5998–6010.

Guza, R. and Thornton, E. (1980). Local an shoaled comparisons of sea surface elevations, pressures, and velocities. *Journal of Geophysical Research*, 85:1524–1530.

Guza, R. and Thornton, E. (1981). Wave set-up on a natural beach. *Journal of Geophysical Research*, 86:4133–4137.

Guza, R. T. and Thornton, E. B. (1982). Swash oscillations on a natural beach. *Journal of Geophysical Research*, 87(C1):483–491.

Holman, R. A. (1983). chapter Edge Waves and the Configuration of the Shoreline. CRC series in marine science. CRC Press, Boca Raton, Fla.

Holman, R. A. (1986). Extreme value statistics for wave run-up on a natural beach. *Coastal Engineering*, 9(6):527–544.

Holman, R. A. and Guza, R. T. (1984). Measuring run-up on a natural beach. *Coastal Engineering*, 8(2):129–140.

Holman, R. A. and Sallenger, A. H. (1985). Setup and Swash on a Natural Beach. *Journal of Geophysical Research*, 90(C1):945–953.

Hughes, M. G., Moseley, A. S., and Baldock, T. E. (2010). Probability distributions for wave runup on beaches. *Coastal Engineering*, 57(6):575–584.

Hunt, I. (1959). Design of seawalls and breakwaters. *Journal of Waterways and Harbours Division*, 85:123–152.

Huntley, D. A. and Bowen, A. J. (1973). Field observations of edge waves. *Nature*, 243(5403):160–162.

Huntley, D. A., Guza, R. T., and Bowen, A. J. (1977). A universal form for shoreline run-up spectra. *Journal of Geophysical Research (1896-1977)*, 82(18):2577–2581.

Häfner, D., Gemmrich, J., and Jochum, M. (2021). FOWD: A free ocean wave dataset for data mining and machine learning. *Journal of Atmospheric and Oceanic Technology*.

Komar, Paul D., . (1998). *Beach processes and sedimentation*. Prentice Hall, Upper Saddle River, N.J, 2nd edition.

Li, C., Özkan-Haller, H., Lomonaco, P., Maddux, T., and García Medina, G. (2022). Experimental study of wave runup variability on a dissipative beach. *Journal of Geophysical Research: Oceans*, 127.

Mansard, E. P. D. and Funke, E. R. (1980). The measurement of incident and reflected spectra using a least squares method. *Coastal Engineering Proceedings*, 1(17):8.

Newell, C., Mullarkey, T., and Clyne, M. (2005). Radiation stress due to ocean waves and the resulting currents and set-up/set-down. In *Ocean Dynamics*, volume 55, pages 499–514. Springer.

Nielsen, P. and Hanslow, D. J. (1991). Wave runup distributions on natural beaches. *J. Coastal Research*, 7(4):1139–1152.

Power, H. E., Gharabaghi, B., Bonakdari, H., Robertson, B., Atkinson, A. L., and Baldock, T. E. (2019). Prediction of wave runup on beaches using gene-expression programming and empirical relationships. *Coastal Engineering*, 144:47–61.

Senechal, N., Dupuis, H., Bonneton, P., Howa, H., Pedreros, R., Sénéchal, N., Dupuis, H., Bonneton, P., Howa, H., and Pedreros, R. (2011). Observation of irregular wave transformation in the surf zone over a gently sloping sandy beach on the french atlantic coastline. *Oceanologica acta*, 24(6):545–556.

Sorensen, R. (2006). *Basic Coastal Engineering: Third Edition*. Number v. 10. Springer US.

Stockdon, H. F., Holman, R. A., Howd, P. A., and Sallenger, A. H. (2006). Empirical parameterization of setup, swash, and runup. *Coastal Engineering*, 53(7):573–588.

Stringari, C. E., Harris, D. L., and Power, H. E. (2019). A novel machine learning algorithm for tracking remotely sensed waves in the surf zone. *Coastal Engineering*, 147:149–158.

Stringari, C. E. and Power, H. E. (2020). Quantifying Bore-Bore Capture on Natural Beaches. *Journal of Geophysical Research: Oceans*, 125(6).

Svendsen, I. (2006). *Introduction to Nearshore Hydrodynamics*. Advanced series on ocean engineering. World Scientific.

Symonds, G., Huntley, D. A., and Bowen, A. J. (1982). Two-dimensional surf beat: long wave generation by a time-varying breakpoint. *Journal of Geophysical Research*, 87(C1):492–498.

Thomson, R. E. (1981). *Oceanography of the British Columbia coast.* Canadian special publication of fisheries and aquatic sciences ; 56. Canada Dept. of Fisheries and Oceans, Ottawa, Ont.

Tissier, M., Bonneton, P., Michallet, H., and Ruessink, B. G. (2015). Infragravity-wave modulation of short-wave celerity in the surf zone. *Journal of Geophysical Research: Oceans*, 120(10):6799–6814.

Webber, N. B. and Bullock, G. N. (1968). A model study of the distribution of run-up of wind-generated waves on sloping sea walls. *Coastal Engineering*, 1:56–56.

Weishar, L. and Byrne, R. (1979). Field study of breaking wave characteristics. *Coastal Engineering Proceedings*, 1:487–506.